

Spatial and Spectral Representations of the Geoid-to-Quasigeoid Correction

Robert Tenzer^{1,2} · Christian Hirt^{3,4} · Sten Claessens³ · Pavel Novák¹

Received: 18 January 2015 / Accepted: 24 August 2015 / Published online: 7 September 2015
© Springer Science+Business Media Dordrecht 2015

Abstract In geodesy, the geoid and the quasigeoid are used as a reference surface for heights. Despite some similarities between these two concepts, the differences between the geoid and the quasigeoid (i.e. the geoid-to-quasigeoid correction) have to be taken into consideration in some specific applications which require a high accuracy. Over the world's oceans and marginal seas, the quasigeoid and the geoid are identical. Over the continents, however, the geoid-to-quasigeoid correction could reach up to several metres especially in the mountainous, polar and geologically complex regions. Various methods have been developed and applied to compute this correction regionally in the spatial domain using detailed gravity, terrain and crustal density data. These methods utilize the gravimetric forward modelling of the topographic density structure and the direct/inverse solutions to the boundary-value problems in physical geodesy. In this article, we provide a brief summary of existing theoretical and numerical studies on the geoid-to-quasigeoid correction. We then compare these methods with the newly developed procedure and discuss some numerical and practical aspects of computing this correction. In global applications, the geoid-to-quasigeoid correction can conveniently be computed in the spectral domain. For this purpose, we derive and present also the spectral expressions for computing this correction based on applying methods for a spherical harmonic analysis and synthesis of global gravity, terrain and crustal structure models. We argue that the newly developed procedure for the regional gravity-to-potential conversion, applied for

✉ Robert Tenzer
rtenzenr@sgg.whu.edu.cn

¹ New Technologies for the Information Society (NTIS), Faculty of Applied Sciences, University of West Bohemia, Plzeň, Czech Republic

² The Key Laboratory of Geospace Environment and Geodesy, School of Geodesy and Geomatics, Wuhan University, 129 Luoyu Road, Wuhan 430079, China

³ Western Australian Geodesy Group and The Institute for Geoscience Research, Curtin University, Perth, Australia

⁴ Institute for Astronomical and Physical Geodesy and Institute for Advanced Study, Technische Universität München, Munich, Germany

computing the geoid-to-quasigeoid correction in the spatial domain, is numerically more stable than the existing inverse models which utilize the gravity downward continuation. Moreover, compared to existing spectral expressions, our definition in the spectral domain takes not only the terrain geometry but also the mass density heterogeneities within the whole Earth into consideration. In this way, the geoid-to-quasigeoid correction and the respective geoid model could be determined more accurately.

Keywords Correction · Geoid · Gravity · Height · Quasigeoid

1 Introduction

The actual distance along the plumbline between the geoid and the topographic surface defines the orthometric height. Since the geoid determination requires the knowledge of mass density distribution within the topography, the mathematical approximation of the Earth by the quasigeoid—free of any hypothetical assumptions on the topographic density distribution—is often used as an alternative concept to the geoid for a definition of height systems. In this case, the normal height is defined as the vertical displacement (along the ellipsoidal normal) of the topographic surface from the quasigeoid. Normal and orthometric heights are thus the most widely used types of heights for geodetic vertical datum realization. These two types of heights can be used if height benchmarks were established based on geodetic spirit levelling and gravity measurements along levelling lines. In some countries, however, gravity values (along levelling lines) were calculated only approximately using normal gravity formulas. The vertical datum is then defined by the normal-orthometric heights (e.g., Meyer et al. 2007).

Asserting that the topographic density and the actual vertical gravity gradient inside the Earth's masses could not be determined precisely, Molodensky (1945, 1948) formulated the theory of normal heights (see also Molodensky et al. 1960). According to this concept the mean gravity (along the plumbline) within the topography is replaced by the mean normal gravity (along the ellipsoidal normal) between the reference ellipsoid and telluroid (see also Heiskanen and Moritz 1967, Chap 4). For a practical realization of the geodetic vertical datum, Helmert's (1884, 1890) orthometric heights are also often used. This method requires only a simple computation of mean gravity by means of applying Poincaré–Prey gravity reduction (e.g., Heiskanen and Moritz 1967, Chap 4-3) while assuming a uniform topographic density distribution. To determine the orthometric heights in mountainous regions with accuracy of a few centimetres or better, Helmert's approximation is not sufficient. Therefore, more accurate methods for the evaluation of mean gravity have to be applied taking the effects of terrain and variable topographic density into consideration. Moreover, mean gravity within the topography depends also on the gravitational effect of mass density heterogeneities distributed below the geoid surface (Tenzer 2004; Tenzer et al. 2005).

In an attempt to improve the accuracy of Helmert's definition, Niethammer (1932, 1939) took the terrain effect into consideration while assuming only a uniform topographic density. According to his method, the mean value of the planar terrain correction is evaluated as a simple average of values computed at the finite number of points along the plumbline within the topography. Mader (1954) estimated a difference between the Helmert and Niethammer methods of ~6 cm for Hochtort (2504 m) in the European Alps (see

also Heiskanen and Moritz 1967, Chap. 4-6). Mader (1954) and Ledersteger (1968) also presupposed that the terrain correction varies linearly with depth. Based on this assumption, the mean terrain correction is averaged from values computed at the topographic surface and at the geoid. Flury and Rummel (2009), however, demonstrated that nonlinear changes of the terrain correction could not be disregarded. Hence, the mean terrain correction should be computed according to Niethammer. Wirth (1990) modified Niethammer's method by means of computing the topographic gravity potential (instead of the terrain correction) at points at the topographic surface and the geoid. The topographic density variation can cause changes of the geoid (and consequently the orthometric heights) up to several decimetres (see Vaniček et al. 1995; Vaniček and Kingdon 2012). The correction to Helmert's orthometric height due to lateral variation of topographic density can be evaluated using a simple formula in which the change of the orthometric height is in a linear relation to the anomalous lateral topographic density (Heiskanen and Moritz 1967). Adopting this relation, the effect of the anomalous topographic density to Helmert's orthometric heights was investigated, for instance, by Allister and Featherstone (2001) and Tenzer and Vaniček (2003). In these approximate definitions of the orthometric height, the vertical gravity gradient generated by mass density heterogeneities distributed below the geoid surface is approximated by the linear normal gravity gradient while disregarding the change of the normal gravity gradient with depth. Hwang and Hsiao (2003) estimated that the errors due to disregarding a nonlinear change of the normal gravity gradient can reach several centimetres in mountainous regions. Tenzer and Vaniček (2003) applied analytical downward continuation of observed gravity in the evaluation of mean gravity based on assuming the lateral topographic density distribution. They then formulated the relation between Poincaré–Prey gravity gradient and the analytical downward continuation of gravity. Kingdon et al. (2009) used the density interfaces as different layers to model the topographic effect in gravimetric geoid determination.

An accurate method for a determination of the integral mean of gravity along the plumbline within the topography was introduced by Tenzer (2004). Following this concept, Tenzer et al. (2005) applied the decomposition of mean gravity into mean normal gravity, the mean no-topography gravity disturbance (generated by the mass density heterogeneities below the geoid surface) and the mean values of the gravitational attraction of topographic and atmospheric masses. Mean normal gravity is then evaluated according to Somigliana–Pizzetti theory of the normal gravity field (Pizzetti 1911; Somigliana 1929). The mean topography-generated gravitational attraction is defined in terms of the difference between gravitational potentials reckoned at the geoid and the topographic surface, multiplied by the reciprocal of the orthometric height. The same principle is applied for a definition of the mean atmosphere-generated gravitational attraction. The mean no-topography gravity disturbance along the plumbline between the geoid and the topographic surface is calculated from the no-topography gravity disturbances at the geoid by applying Poisson's integral. Prior to this numerical step, the no-topography gravity disturbances at the topographic surface have to be downward continued to the geoid by solving the inverse to Dirichlet's boundary-value problem. Santos et al. (2006) compared the differences between various orthometric height definitions. In addition to the above theoretical developments, numerous empirical studies were published on the orthometric height definition (e.g., Ledersteger 1955; Rapp 1961; Krakiwsky 1965; Strange 1982; Sünkel 1986; Kao et al. 2000; Drewes et al. 2002; Dennis and Featherstone 2003; Featherstone and Kuhn 2006).

In recent years, a considerable effort has been undertaken to unify a large number of existing vertical datum realizations around the world. The vertical datum unification typically requires the joint adjustment of interconnected levelling networks and/or the

estimation of the vertical datum offset with respect to the World Height System (WHS) which is defined by the geoidal geopotential value W_0 (cf. Burša et al. 1997, 1999). The estimated values of W_0 were reported by Burša et al. (1997, 2007), Sanchez (2007) and Dayoub et al. (2012). Alternatively, vertical datum unification can be realized though the gravimetric determination of the global geoid/quasigeoid model with a high accuracy and spatial resolution. Since the geodetic vertical controls worldwide are defined using different types of heights and every country has adopted their own height system specifications, the precise conversion between different height systems is inevitable.

Height conversion has been addressed extensively in geodetic literature. An approximate formula relating the (Molodensky) normal and (Helmert) orthometric heights was given, for instance, in Heiskanen and Moritz (1967, Eq. 8–103). According to this formula, the geoid-to-quasigeoid correction is defined as a function of the simple planar Bouguer gravity anomaly and the topographic height. Sjöberg (1995) slightly improved the classical definition by adding a small term related to the vertical derivative of the gravity anomaly. Rapp (1997) formulated the computation of the geoid-to-quasigeoid correction in spherical harmonics and applied the approach with the Earth's gravitational models (EGMs). Tenzer et al. (2005) presented numerical procedures for a rigorous computation of the orthometric height and formulated an accurate relation between the (rigorous) orthometric and normal heights. An alternative method of computing the geoid-to-quasigeoid correction was given by Tenzer et al. (2006). They derived this correction by comparing the geoidal height and the height anomaly, both defined by Brun's (1878) theorem. It is important to note that the height anomaly is defined as the vertical displacement (along the ellipsoidal normal) between the telluroid and the topographic surface. Consequently, the vertical displacement between the ellipsoid and the telluroid defines the normal height (e.g., Heiskanen and Moritz 1967, Chap 8–3). Since this theoretical definition is not convenient for practical purposes, the normal height is formally considered as the vertical distance between the quasigeoid and the topographic surface and the quasigeoidal height is measured from the ellipsoid surface (see Fig. 1). Obviously, the quasigeoidal height and the height anomaly are equal. A very similar expression for computing the geoid-to-quasigeoid correction was given by Sjöberg (2006). The definitions of the geoid-to-quasigeoid correction presented

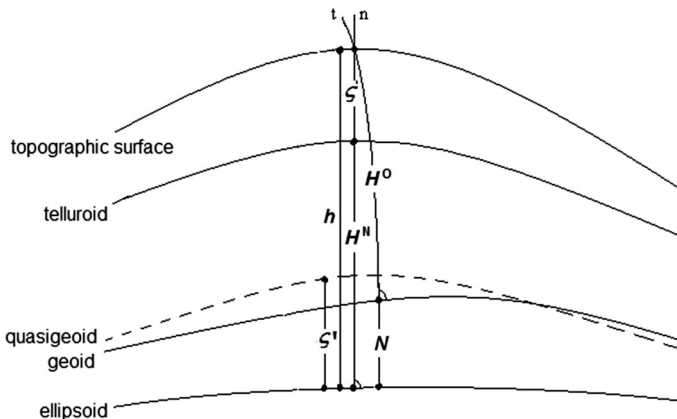


Fig. 1 Height systems: the normal height H^N , the orthometric height H^O , the geodetic (ellipsoidal) height h , the geoidal height N , the height anomaly ζ' , and the quasigeoidal height ζ' . The plumline and ellipsoidal normal are denoted as t and n respectively

by Tenzer et al. (2005, 2006) and Sjöberg (2006) incorporated information on the terrain geometry, variable topographic density and mass density heterogeneities distributed below the geoid surface. Flury and Rummel (2009) demonstrated that the consideration of terrain significantly reduces the values of the geoid-to-quasigeoid correction computed using the classical definition in which the topography is approximated by the Bouguer plate. The results of Flury and Rummel (2009) were in a good agreement with previous results over a larger area in the European Alps presented by Marti (2005) and Sünkel et al. (1987), see also Hofmann-Wellenhof and Moritz (2005, Chap 4). Following the work of Flury and Rummel (2009), Sjöberg (2010) derived a slightly more accurate expression for the geoid-to-quasigeoid correction, consistent with a definition of the boundary condition of physical geodesy. He, however, also stated that his more refined expression could improve the accuracy not more than ~ 1 cm compared to the expression given by Flury and Rummel (2009). Later, Sjöberg (2012) applied an arbitrary compensation model in computing the topographic correction term. In particular, he recommended using either the Helmert or isostatic types of reductions, which provide smaller and smoother components, more suitable for interpolation and calculation, than the Bouguer reduction. Hirt (2012) refined parts of Rapp's (1997) computational approach by introducing higher-order terms in the harmonic synthesis which are relevant for the computation of the geoid-to-quasigeoid correction from high-degree EGMs.

It is worth mentioning that some authors developed and applied methods for the conversion of the normal-orthometric to normal heights. Filmer et al. (2010), for instance, applied the cumulative normal to normal-orthometric height correction in the Australian Height Datum. They used the EGM2008 (Pavlis et al. 2012) to reconstruct observed gravity data at levelling benchmarks of the Australian National Levelling Network. According to their method, the normal to normal-orthometric height correction along levelling lines was calculated cumulatively as a sum of the product of the levelled height differences and the surface values of the gravity disturbances. Tenzer et al. (2011a, 2011b) defined this correction more rigorously as a function of gravity anomalies instead of gravity disturbances, because the normal gravity at the topographic surface (in the definition of the normal potential number) is calculated for the levelled heights (and not for the geodetic heights). They applied this correction in the (experimental) unification of the local vertical controls (LVDs) at the North and South Islands of New Zealand.

Although numerous studies have been addressing theoretical and practical aspects of the geoid and quasigeoid determination, the differences between them are often disregarded. One example can be given in geophysical applications where the EGM coefficients are used to compute the geoid model globally. Since the EGMs describe the external gravitational field of the Earth, the “true” geoid can directly be recovered from EGMs only over the world's oceans and marginal seas and possibly also over low-elevated continental regions where the differences between the geoid and the quasigeoid are negligible or below the accuracy required for a particular application. In the mountainous, polar and geologically complex regions, however, the geoid could only be determined realistically if additional information on the terrain geometry is taken into consideration. Moreover, mantle density heterogeneities, continental polar ice sheets and large continental sedimentary basins significantly affect the long-to-medium wavelengths of the Earth's equipotential geometry and consequently also the respective long-wavelength harmonic spectrum of the geoid-to-quasigeoid correction.

In this study, we address these aspects and present the complete numerical methods for computing the geoid-to-quasigeoid correction in the spatial and spectral domains. For this purpose, we first derive a rigorous formula for the geoid-to-quasigeoid correction in

Sect. 2. We then present numerical procedures for an accurate computation of the geoid-to-quasigeoid correction in the spatial domain and compare these procedures with published methods in Sect. 3. These numerical procedures are suitable especially for local or regional applications. In global applications, the computation of this correction is typically realized in a frequency domain to a certain degree of spectral resolution. The expressions for computing this correction in the spectral domain are derived and presented in Sect. 4. Some practical aspects of computing the geoid-to-quasigeoid correction are discussed in Sect. 5. The summary and concluding remarks are given in Sect. 6. The focus of our study is on the derivation of computational formalisms, while the application of these numerical methods on synthetic or real data is out of the scope of this study.

2 Geoid-to-Quasigeoid Correction

The geoidal height N is defined by (e.g., Heiskanen and Moritz 1967, Eq. 2–144)

$$N(\Omega) = \frac{T(r_g, \Omega)}{\gamma_0(\phi)}, \quad (1)$$

where the disturbing potential T (i.e. the difference between the actual and normal gravity potentials) is stipulated at the geoid surface (r_g, Ω) of which the geocentric radius is r_g , and $\Omega = (\phi, \lambda)$ is the spherical direction with the spherical latitude ϕ and longitude λ . The normal gravity γ_0 in Eq. (1) is evaluated at the reference ellipsoid typically according to the Geodetic Reference System 1980 (GRS80) parameters (Moritz 2000).

Molodensky (1945, 1948) defined the height anomaly ζ as follows (see also Molodensky et al. 1960; Heiskanen and Moritz 1967, Eqs. 8–10)

$$\zeta(\Omega) = \frac{T(r_t, \Omega)}{\gamma(H^N, \phi)}, \quad (2)$$

where the disturbing potential T is in this case stipulated at the topographic surface (r_t, Ω) of which the geocentric radius is denoted as r_t . The normal gravity γ in Eq. (2) is evaluated at the telluroid (H^N, ϕ) which is vertically displaced from the reference ellipsoid by the normal height H^N .

From Eqs. (1) and (2), the geoid-to-quasigeoid correction χ is obtained in the following form

$$\chi(\Omega) = N(\Omega) - \zeta(\Omega) = \frac{T(r_g, \Omega)}{\gamma_0(\phi)} - \frac{T(r_t, \Omega)}{\gamma(H^N, \phi)}. \quad (3)$$

Errors due to disregarding the nonlinear terms in definitions of the geoidal height and the height anomaly in Eqs. (1) and (2) by means of applying Bruns's theorem cause uncertainties in the geoid-to-quasigeoid correction in Eq. (3) not more than 1.5 mm (cf. Sjöberg 2006).

After some algebra, Eq. (3) is rewritten as

$$\begin{aligned} \chi(\Omega) &= \frac{1}{\gamma_0(\phi)} [T(r_g, \Omega) - T(r_t, \Omega)] + \frac{T(r_t, \Omega)}{\gamma(H^N, \phi)} \left[\frac{\gamma(H^N, \phi)}{\gamma_0(\phi)} - 1 \right] \\ &= \frac{1}{\gamma_0(\phi)} [T(r_g, \Omega) - T(r_t, \Omega)] + \zeta(\Omega) \frac{\gamma(H^N, \phi) - \gamma_0(\phi)}{\gamma_0(\phi)}. \end{aligned} \quad (4)$$

The geoid-to-quasigeoid correction in Eq. (4) is described by the two constituents related to the disturbing potential difference and the normal gravity difference. The former represents a major contribution to χ . The latter is further defined in terms of the normal vertical gravity gradient. A similar definition of χ was given before by Tenzer et al. (2006) using a Taylor series to define the normal gravity difference. We note here that Eq. (3) and all expressions hereafter actually define the geoid-to-quasigeoid correction as negative, because the value χ has to be added to the height anomaly in order to obtain the geoidal height, i.e. $N = \varsigma + \chi$.

If we disregard the nonlinear changes in the vertical normal gravity gradient, i.e.

$$\gamma(H^N, \phi) \approx \gamma_0(\phi) + \left. \frac{\partial \gamma}{\partial h} \right|_{h=0} H^N(\Omega), \tag{5}$$

the second constituent on the right-hand side of Eq. (4) becomes

$$\varsigma(\Omega) \frac{\gamma(H^N, \phi) - \gamma_0(\phi)}{\gamma_0(\phi)} \cong \frac{1}{\gamma_0(\phi)} \left. \frac{\partial \gamma}{\partial h} \right|_{h=0} H^N(\Omega) \varsigma(\Omega), \tag{6}$$

where h is the geodetic height. Substituting $\gamma_0 \approx GM/R^2$ and $\partial \gamma / \partial h \approx -2GM/R^3$ in Eq. (6), we get

$$\varsigma(\Omega) \frac{\gamma(H^N, \phi) - \gamma_0(\phi)}{\gamma_0(\phi)} \approx -\frac{2GM}{R^3} \frac{R^2}{GM} H^N(\Omega) \varsigma(\Omega) = -\frac{2}{R} H^N(\Omega) \varsigma(\Omega), \tag{7}$$

where $GM = 3986005 \times 10^8 \text{ m}^3 \text{ s}^{-2}$ is the geocentric gravitational constant, and $R = 6371 \times 10^3 \text{ m}$ is the Earth’s mean radius. Setting $H \approx 8.85 \times 10^3 \text{ m}$ and $\varsigma \approx \pm 100 \text{ m}$, the second constituent on the right-hand side of Eq. (4) will not exceed a maximum of $\pm 0.3 \text{ m}$. The errors due to disregarding the nonlinear changes of the normal gravity gradient in Eq. (5) are less than 1 mm. This is evident from $(2\gamma_0)^{-1} H^2 \varsigma \partial^2 \gamma / \partial h^2 \approx H^2 \varsigma / 3R^2$, where $\partial^2 \gamma / \partial h^2 \approx 6GM/R^4$.

To evaluate the first constituent on the right-hand side of Eq. (4), we define the disturbing potential T as a function of the gravity disturbance δg , i.e. $\delta g \cong -\partial T / \partial r$. We then write

$$T(r_g, \Omega) - T(r_t, \Omega) = \int_{r=r_g}^{r_t} \delta g(r, \Omega) \cos(-\mathbf{g}, \mathbf{r}^o) dr \cong \int_{r=r_g}^{r_t} \delta g(r, \Omega) dr, \tag{8}$$

where $\cos(-\mathbf{g}, \mathbf{r}^o)$ is the cosine of the deflection of the plumbline from the geocentric radial direction, \mathbf{g} is the vector of gravity, and \mathbf{r}^o is the unit vector in the geocentric radial direction. Tenzer et al. (2005) demonstrated that neglecting the deflection of the plumbline from the geocentric radial direction, i.e. $\cos(-\mathbf{g}, \mathbf{r}^o) \approx 1$, could increase the error in the orthometric height only by a few millimetres. The integral mean of the gravity disturbance $\overline{\delta g}(\Omega)$ reads (Tenzer 2004)

$$\overline{\delta g}(\Omega) \cong \frac{1}{H^0(\Omega)} \int_{r=r_g}^{r_t} \delta g(r, \Omega) dr, \tag{9}$$

where H^O is the orthometric height. From Eqs. (8) and (9), we get

$$T(r_g, \Omega) - T(r_t, \Omega) = H^O(\Omega) \overline{\delta g}(\Omega). \quad (10)$$

Substituting Eqs. (7) and (10) in Eq. (4), the geoid-to-quasigeoid correction is found to be

$$\begin{aligned} \chi(\Omega) &\cong \frac{T(r_g, \Omega) - T(r_t, \Omega)}{\gamma_0(\phi)} - \frac{2}{R} H^N(\Omega) \zeta(\Omega) \\ &\cong \frac{1}{\gamma_0(\phi)} H^O(\Omega) \overline{\delta g}(\Omega) - \frac{2}{R} H^N(\Omega) \zeta(\Omega) \end{aligned} \quad (11)$$

The orthometric height in Eq. (11) can be replaced by the normal height, and vice versa, without any significant influence on the accuracy; for $H^O - H^N = \pm 5$ m and $\overline{\delta g} = 500$ mGal, the error of χ is only ~ 2.5 mm. The expression in Eq. (11) can then be described in terms of the topographic height H (instead of specifically for H^N or H^O). Hence

$$\chi(\Omega) \cong \frac{H(\Omega)}{\gamma_0(\phi)} \left[\overline{\delta g}(\Omega) - \frac{2}{R} \zeta(\Omega) \gamma_0(\phi) \right]. \quad (11a)$$

Since the second constituent on the right-hand side of Eq. (11a) can readily be computed from the known values of ζ and H , the computational procedure is now reduced to evaluate the integral mean of the gravity disturbance $\overline{\delta g}$. As seen in Eq. (10), the computation of $\overline{\delta g}$ in Eq. (11a) can be done in terms of the disturbing potential difference. In the next section, we present various methods for computing the disturbing potential difference in the spatial domain.

3 Computation in the Spatial Domain

The disturbing potential difference can be evaluated from the observed gravity disturbances/anomalies by applying four (successive) numerical steps comprising: (1) the forward modelling of the topographic gravity correction, (2) the inverse solution to discretized Green's integral equations, (3) the solution to discretized Poisson's integral equation, and (4) the forward modelling of the topographic potential difference.

To better explain these four numerical steps, we first clarify their purpose. By analogy with the gravimetric geoid determination, the gravitational contribution of topographic masses has to be removed from the observed gravity data. For this reason, the forward modelling is applied to compute the topographic gravity correction. In the second step, the topography-corrected gravity data at (or above) the topographic surface are converted to the disturbing potential values at the geoid by solving the inverse to discretized Green's integrals. Subsequently, the disturbing potential values at the geoid are upward continued to the topographic surface by solving the discretized Poisson's integral equation. The disturbing potential values at the geoid and the topographic surface are then used to compute the disturbing potential difference. There is, however, a remaining problem related to the fact that the gravitational contribution of topographic masses was subtracted from the observed gravity data (in the first step) prior to their conversion to potential values (the second and third steps). The disturbing potential values obtained from these gravity data thus do not comprise the topographic effect. Since the integral mean of gravity disturbance is defined inside the topography, the gravitational contribution of topographic

masses has to be restored. This is done by applying the topographic correction to the disturbing potential difference. For this purpose, the forward modelling is used in the final step to compute the topographic potentials at the geoid and the topographic surface. Mathematical formalisms applied for solving these numerical steps using either the gravity disturbances or the gravity anomalies are reviewed below. This numerical procedure is then compared with published methods. The schematic diagrams of these numerical procedures are shown in Fig. 2.

By analogy with the procedure described in Tenzer et al. (2005), we first separate the disturbing potential T into the components which can be calculated separately from gravity data and available terrain and crustal density models. We then write

$$T(r, \Omega) = V^T(r, \Omega) + T^{NT}(r, \Omega), \tag{12}$$

where V^T is the topographic potential, and T^{NT} is the no-topography disturbing potential (Vaníček et al. 2005) which is generated by the mass density heterogeneities distributed below the geoid surface. As seen in Eq. (12), the no-topography disturbing potential can be obtained from the disturbing potential after subtracting the topographic potential. In the

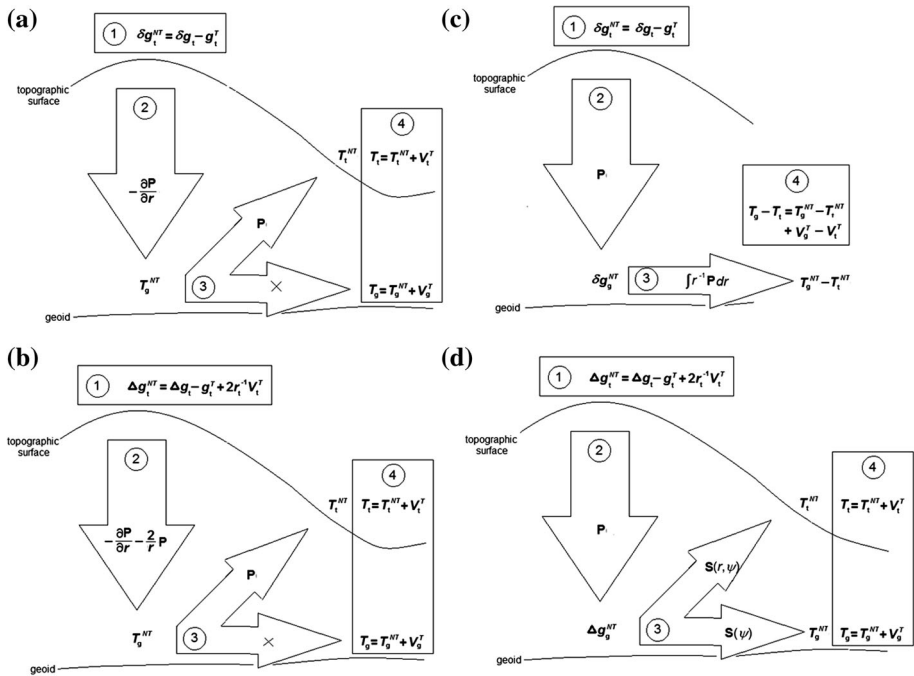


Fig. 2 Numerical procedures applied for computing the geoid-to-quasigeoid correction in the regional gravity inversion: the computation of the disturbing potential difference from the observed gravity disturbances (a) and from the topography-corrected gravity anomalies (b) based on solving the inverse to Green’s integral equation with a subsequent solution to the Poisson’s integral equation. The computation of the disturbing potential difference from the observed gravity disturbances based on solving the inverse to Poisson’s integral equation with a subsequent solution to the radially integrated Poisson’s integral according to Tenzer et al. (2005) (c). The computation of the disturbing potential difference from the observed gravity anomalies based on solving the inverse to Poisson’s integral equation with a subsequent solution to the generalized Stokes’s problem according to Tenzer et al. (2006) and Sjöberg (2006) (d). Note that the values at the geoid and the topographic surface are denoted by subscripts “g” and “t”, respectively

most general case, the atmospheric potential should also be taken into consideration in Eq. (12). Tenzer et al. (2005) demonstrated, however, that the atmospheric effect on the geoid-to-quasigeoid correction is less than 1 mm and thus completely negligible.

We further separate the topographic potential in Eq. (12) into the components $V^{T,\bar{\rho}^T}$ and $V^{T,\delta\rho^T}$ which are related to the constant and anomalous topographic density distribution, i.e. $\bar{\rho}^T = \text{const.}$ and $\delta\rho^T = \rho^T - \bar{\rho}^T$, where ρ^T is the actual topographic density. Hence

$$V^T(r, \Omega) = V^{T,\bar{\rho}^T}(r, \Omega) + V^{T,\delta\rho^T}(r, \Omega). \quad (13)$$

Substituting Eqs. (12) and (13) in Eq. (10), we arrive at

$$T(r_g, \Omega) - T(r_t, \Omega) \cong \left[V^{T,\bar{\rho}^T}(r_g, \Omega) - V^{T,\bar{\rho}^T}(r_t, \Omega) \right] + \left[V^{T,\delta\rho^T}(r_g, \Omega) - V^{T,\delta\rho^T}(r_t, \Omega) \right] + \left[T^{NT}(r_g, \Omega) - T^{NT}(r_t, \Omega) \right]. \quad (14)$$

Whereas the topographic potentials $V^{T,\bar{\rho}^T}$ and $V^{T,\delta\rho^T}$ in Eq. (14) can directly be computed from terrain and crustal density models by applying forward modelling, the evaluation of the no-topography disturbing potential difference from the observed gravity data requires the removal of topographic effect (i.e. the first numerical step) followed by the gravity-to-potential conversion of the non-topographic part of the gravity field (the second step) with the additional upward continuation (the third step).

The no-topography gravity disturbances δg^{NT} at the topographic surface are obtained from the observed gravity disturbances δg after applying the direct topographic effect

$$\delta g^{NT}(r_t, \Omega) = \delta g(r_t, \Omega) - g^{T,\bar{\rho}^T}(r_t, \Omega) - g^{T,\delta\rho^T}(r_t, \Omega), \quad (15)$$

where the topographic attraction g^T consists of two components $g^{T,\bar{\rho}^T}$ and $g^{T,\delta\rho^T}$ which are evaluated again for the reference and anomalous topographic density distribution.

The computation of the no-topography gravity anomalies Δg^{NT} from the observed gravity anomalies Δg is realized by applying the direct and secondary indirect topographic effects (Vaniček et al. 2005)

$$\Delta g^{NT}(r_t, \Omega) = \Delta g(r_t, \Omega) - g^{T,\bar{\rho}^T}(r_t, \Omega) - g^{T,\delta\rho^T}(r_t, \Omega) + \frac{2}{r_t(\Omega)} V^{T,\bar{\rho}^T}(r_t, \Omega) + \frac{2}{r_t(\Omega)} V^{T,\delta\rho^T}(r_t, \Omega). \quad (16)$$

As seen in Eqs. (15) and (16), the direct and secondary indirect topographic effects are defined as g^T and $2r^{-1}V^T$, respectively. We note here that the definitions of δg^{NT} and Δg^{NT} formally also include the respective atmospheric effects. Since the atmospheric effect on the geoid-to-quasigeoid correction is negligible, the atmospheric gravitational effect was not subtracted from the gravity disturbance/anomaly in Eqs. (15) and (16).

3.1 Topographic Component

The topographic potential $V^{T,\bar{\rho}^T}$ is evaluated at a point (r, Ω) by solving Newton's volumetric integral (e.g., Martinec 1998, Chap 3)

$$V^{T,\bar{\rho}^T}(r, \Omega) \cong G\bar{\rho}^T \iiint_{\phi} \int_{r'=R}^{R+H'} \ell^{-1}(r, \psi, r') r'^2 dr' d\Omega', \quad (17)$$

where $G = 6.674 \times 10^{-11} \text{ m}^3 \text{ kg}^{-1} \text{ s}^{-2}$ is the Newton gravitational constant, ℓ is the Euclidean spatial distance between two points (r, Ω) and (r', Ω') , ψ is the respective spherical distance, $d\Omega' = \cos \phi' d\phi' d\lambda'$ is the infinitesimal surface element, and $\phi = \left\{ \Omega' = (\phi', \lambda') : \phi' \in [-\pi/2, \pi/2] \wedge \lambda' \in [0, 2\pi) \right\}$ is the full spatial angle. The reference topographic density of $\bar{\rho}^T = 2670 \text{ kg m}^{-3}$ is typically attributed to an average density of the upper continental crust (cf. Hinze 2003).

By analogy with Eq. (17), we define the topographic potential $V^{T, \delta\rho^T}$ generated by the anomalous topographic density $\delta\rho^T$ in the following form (e.g., Martinec 1998, Chap 6)

$$V^{T, \delta\rho^T}(r, \Omega) \cong G \iint_{\phi} \int_{r=R}^{R+H'} \delta\rho^T(r', \Omega') \ell^{-1}(r, \psi, r') r'^2 dr' d\Omega'. \tag{18}$$

The topographic attractions $g^{T, \bar{\rho}^T}$ and $g^{T, \delta\rho^T}$ (defined approximately as a negative radial derivative of the respective topographic potentials $V^{T, \bar{\rho}^T}$ and $V^{T, \delta\rho^T}$) are given by

$$g^{T, \bar{\rho}^T}(r, \Omega) \cong -\frac{\partial V^{T, \bar{\rho}^T}}{\partial r} \cong -G \bar{\rho}^T \iint_{\phi} \int_{r=R}^{R+H'} \frac{\partial \ell^{-1}(r, \psi, r')}{\partial r} r'^2 dr' d\Omega', \tag{19}$$

and

$$g^{T, \delta\rho^T}(r, \Omega) \cong -\frac{\partial V^{T, \delta\rho^T}}{\partial r} \cong -G \iint_{\phi} \int_{r=R}^{R+H'} \delta\rho^T(r', \Omega') \frac{\partial \ell^{-1}(r, \psi, r')}{\partial r} r'^2 dr' d\Omega'. \tag{20}$$

In Eqs. (17–20) and all equations hereafter, we apply the spherical approximation (i.e. the geocentric radii of the geoid surface are approximated by the Earth’s mean radius). Relative errors of about 0.3 % are to be expected in the computed gravity field quantities due to disregarding the Earth’s flattening (cf. Heiskanen and Moritz 1967, Chap 2–14). Moreover, strict definition of the height system (i.e. either the orthometric or normal heights) is not required in computing the geoid-to-quasigeoid correction, because topographic information is typically retrieved from digital terrain models (DTMs). Hence, we refer here to the topographic height H instead of specifically to H^N or H^O . The geocentric radii of the topographic surface and the geoid are then defined as $r_t \cong R + H$ and $r_g \cong R$, respectively, and the radial integration is within the interval of: $R \leq r' \leq R + H'$.

3.2 Non-topographic Component

The computation of the non-topographic part of the geoid-to-quasigeoid correction is realized in two steps (see Figs. 2a, b). First, the harmonic downward continuation is applied by means of solving the inverse to discretized Green’s integral equations. In this numerical step, the values of T^{NT} are determined at the geoid from the values of δg^{NT} or Δg^{NT} at the topographic surface. The Green integrals read (Novák 2003; Tenzer and Novák 2008)

$$r \delta g^{NT}(r, \Omega) = -\frac{r}{4\pi} \iint_{\phi} \frac{\partial P(r, \psi, R)}{\partial r} T^{NT}(r'_g, \Omega') d\Omega' \quad (r \geq R), \tag{21}$$

and

$$r \Delta g^{NT}(r, \Omega) = -\frac{r}{4\pi} \iint_{\phi} \left[\frac{\partial P(r, \psi, R)}{\partial r} + \frac{2}{r} P(r, \psi, R) \right] T^{NT}(r'_g, \Omega') d\Omega' \quad (r \geq R), \tag{22}$$

where P is the Poisson kernel (e.g., Heiskanen and Moritz 1967, Chap 1–16). We note here that the products $r\delta g^{NT}$ and $r\Delta g^{NT}$ are harmonic functions everywhere above the geoid, i.e. $\forall r > R : \Delta(r\delta g^{NT}) = 0$ and $\forall r > R : \Delta(r\Delta g^{NT}) = 0$. The harmonic upward continuation, realized by solving the discretized Poisson’s integral equation, is then applied to evaluate the no-topography disturbing potential T^{NT} at the topographic surface. The Poisson integral reads (e.g., Heiskanen and Moritz 1967, Eq. 1-88)

$$T^{NT}(r, \Omega) = \frac{1}{4\pi} \iint_{\phi} P(r, \psi, R) T^{NT}(r'_g, \Omega') d\Omega' \quad (r \geq R). \tag{23}$$

For $r \geq R$, the Poisson kernel P and the respective Green kernels $\partial P / \partial r$ and $\partial P / \partial r + 2P/r$ in Eqs. (21–23) are given by (e.g., Tenzer and Novák 2008)

$$P(r, \psi, R) = R \frac{r^2 - R^2}{\ell^3(r, \psi, R)}, \tag{24}$$

$$\frac{\partial P(r, \psi, R)}{\partial r} = \frac{2rR}{\ell^3(r, \psi, R)} - 3R \frac{r^2 - R^2}{\ell^5(r, \psi, R)} (r - R \cos \psi), \tag{25}$$

$$\frac{\partial P(r, \psi, R)}{\partial r} + \frac{2}{r} P(r, \psi, R) = \frac{2R}{r} \frac{r^2 - R^2}{\ell^3(r, \psi, R)} - 3R \frac{r^2 - R^2}{\ell^5(r, \psi, R)} (r - R \cos \psi). \tag{26}$$

An alternative approach for computing the no-topography disturbing potential difference was proposed by Tenzer et al. (2005). They applied the downward continuation of the no-topography gravity disturbances based on solving the inverse to discretized Poisson’s integral equations. The resulting no-topography gravity disturbances at the geoid are then used to evaluate the radial integral of discretized Poisson’s integral equation (see Fig. 2c). The Poisson integral for δg^{NT} reads

$$r\delta g^{NT}(r, \Omega) = \frac{R}{4\pi} \iint_{\phi} P(r, \psi, R) \delta g^{NT}(r'_g, \Omega') d\Omega' \quad (r \geq R). \tag{27}$$

The radial integral of Poisson’s integral is given by (Tenzer et al. 2005)

$$\begin{aligned} T^{NT}(r_g, \Omega) - T^{NT}(r_t, \Omega) &\cong \int_{r=R}^{R+H} \delta g^{NT}(r, \Omega) dr \\ &= \frac{R}{4\pi} \iint_{\phi} \int_{r=R}^{R+H} r^{-1} P(r, \psi, R) dr \delta g^{NT}(r'_g, \Omega') d\Omega' \quad (r \geq R), \end{aligned} \tag{28}$$

where

$$\int_r r^{-1} P(r, \psi, R) dr = -2R\ell^{-1}(r, \psi, R) + \ln \left| \frac{R - r \cos \psi + \ell(r, \psi, R)}{r \sin \psi} \right|. \tag{29}$$

It is worth mentioning that the computation of the (no-topography) disturbing potential difference from the respective gravity disturbances at the geoid can be realized by applying Hotine’s integrals (e.g., Featherstone 2013).

Since gravity anomalies are until now the most commonly used gravity data type, it is convenient to compute the geoid-to-quasigeoid correction from the observed gravity anomalies without their additional conversion to gravity disturbances. Such a procedure was discussed in Tenzer et al. (2006) and Sjöberg (2006). According to their approach, the no-topography gravity anomalies (defined in Eq. 16) are first downward continued onto the geoid. This numerical step is realized by solving the inverse to discretized Poisson's integral. By analogy with Eq. (27), the Poisson integral for Δg^{NT} reads

$$r\Delta g^{NT}(r, \Omega) = \frac{R}{4\pi} \iint_{\phi} P(r, \psi, R) \Delta g^{NT}(r'_g, \Omega') d\Omega' \quad (r \geq R). \quad (30)$$

In the second step, the no-topography gravity anomalies at the geoid (obtained after solving Eq. 30) are used to compute the no-topography disturbing potential values at the topographic surface and the geoid, yielding the (no-topography) disturbing potential difference (see Fig. 2d). This is done by solving the generalized Stokes's problem (Tenzer et al. 2006; Sjöberg 2006)

$$T^{NT}(r_g, \Omega) - T^{NT}(r_t, \Omega) \cong \frac{R}{4\pi} \iint_{\phi} [S(\psi) - S(r, \psi)] \Delta g^{NT}(r'_g, \Omega') d\Omega', \quad (31)$$

where the closed analytical formulas of the Stokes kernels $S(\psi)$ and $S(r, \psi)$ are given by (cf. Heiskanen and Moritz 1967, Eqs. 2-164 and 2-162)

$$S(\psi) = \cos \operatorname{ec} \frac{\psi}{2} - 6 \sin \frac{\psi}{2} + 1 - 5 \cos \psi - 3 \cos \psi \ln \left(\sin \frac{\psi}{2} + \sin^2 \frac{\psi}{2} \right), \quad (32)$$

and

$$S(r, \psi) = \frac{2R}{\ell(r, \psi, R)} + \frac{R}{r} - 3 \frac{R}{r^2} \ell(r, \psi, R) - \left(\frac{R}{r} \right)^2 \cos \psi \left[5 + 3 \ln \frac{r - R \cos \psi + \ell(r, \psi, R)}{2r} \right]. \quad (33)$$

Whereas the gravity-to-potential conversion of the non-topographic part of the gravity field is realized through the downward continuation procedure of solving the inverse to discretized Green's integral equations (Eqs. 21 and 22), in the alternative approaches this conversion is realized after the gravity downward continuation by solving either the radial integral of discretized Poisson's integral equation for the values of δg^{NT} (Eq. 28) or the generalized Stokes's problem for the values of Δg^{NT} (Eq. 31). In the final step, the disturbing potential difference is obtained from the respective non-topographic value by adding the topographic potential difference (see Eq. 14). The computation of the topographic potential difference can be realized by solving either Newton's volumetric integral for the potential values or the radial integral of Newton's integral for the topographic attraction. A more detailed discussion of solving Newton's integral in the spatial domain is out of the scope of this study while focusing only on its evaluation in the spectral domain.

4 Computation in the Spectral Domain

In this section, we introduce the expressions for computing the geoid-to-quasigeoid correction in the spectral domain based on methods for the spherical analysis and synthesis of the gravity field and using terrain and crustal density models. With reference to the

decomposition of the disturbing potential difference in Eq. (14), we derive the spectral expressions individually for the topographic potential differences of reference and anomalous density distributions and for the no-topography disturbing potential.

4.1 Topographic Potential Difference (of Reference Density)

We express the topographic potential difference (in the first constituent on the right-hand side of Eq. 14) by means of applying the analytical downward continuation of the topographic potential $V_e^{T,\bar{\rho}^T}$ (which is defined for the external convergence domain) and introducing the topographic bias. Sjöberg (2007) defined the topographic bias as the difference between the downward-continued gravitational potential $\lim_{r \rightarrow R^-} V_e^{T,\bar{\rho}^T}(r, \Omega)$ (for the external convergence domain) and the topographic potential computed for the internal convergence domain $\lim_{r \rightarrow R^-} V_i^{T,\bar{\rho}^T}(r, \Omega)$. The analytical downward continuation is in this case permissible due to assuming a constant topographic density and can also be applied for a density distribution with only lateral variations. The topographic potential difference then takes the following form

$$\begin{aligned} V_e^{T,\bar{\rho}^T}(r_g, \Omega) - V_e^{T,\bar{\rho}^T}(r_t, \Omega) &= \lim_{r \rightarrow R^-} V_i^{T,\bar{\rho}^T}(r, \Omega) - V_e^{T,\bar{\rho}^T}(r_t, \Omega) \\ &= \lim_{r \rightarrow R^+} V_e^{T,\bar{\rho}^T}(r, \Omega) - V_e^{T,\bar{\rho}^T}(r_t, \Omega) \\ &\quad + \lim_{r \rightarrow R^-} V_i^{T,\bar{\rho}^T}(r, \Omega) - \lim_{r \rightarrow R^+} V_e^{T,\bar{\rho}^T}(r, \Omega), \end{aligned} \tag{34}$$

where $V_e^{T,\bar{\rho}^T}(r_t, \Omega) - \lim_{r \rightarrow R^+} V_e^{T,\bar{\rho}^T}(r, \Omega)$ is the analytical continuation term, and $\lim_{r \rightarrow R^+} V_e^{T,\bar{\rho}^T}(r, \Omega) - \lim_{r \rightarrow R^-} V_i^{T,\bar{\rho}^T}(r, \Omega)$ is the topographic bias. The spectral form of the topographic potential $V_e^{T,\bar{\rho}^T}$ for the external convergence domain is derived in ‘‘Appendix 1’’.

From Eq. (63), the topographic potential $V_e^{T,\bar{\rho}^T}$ at the topographic surface, i.e. $r_t = R + H$, is computed as follows

$$\begin{aligned} V_e^{T,\bar{\rho}^T}(r_t, \Omega) &\cong 4\pi G \bar{\rho}^T R^2 \sum_{n=0}^{\infty} \left(\frac{R}{R+H}\right)^{n+1} \frac{1}{2n+1} \\ &\quad \times \sum_{k=0}^{n+2} \binom{n+2}{k} \frac{1}{R^{k+1}} \frac{1}{k+1} \sum_{m=-n}^n H_{n,m}^{(k+1)} Y_{n,m}(\Omega), \end{aligned} \tag{35}$$

where $Y_{n,m}$ are the surface spherical harmonics. The Laplace harmonics H_n of the topographic heights (including their higher-order terms) are defined in Eqs. (61) and (62).

The analytically continued value of $V_e^{T,\bar{\rho}^T}$ at the geoid, i.e. $r = R$, is given by

$$\begin{aligned} \lim_{r \rightarrow R^+} V_e^{T,\bar{\rho}^T}(r, \Omega) &\cong 4\pi G \bar{\rho}^T R^2 \sum_{n=0}^{\infty} \frac{1}{2n+1} \\ &\quad \times \sum_{k=0}^{n+2} \binom{n+2}{k} \frac{1}{R^{k+1}} \frac{1}{k+1} \sum_{m=-n}^n H_{n,m}^{(k+1)} Y_{n,m}(\Omega). \end{aligned} \tag{36}$$

From Eqs. (35) and (36), the (negative) analytical continuation term becomes

$$\begin{aligned} \lim_{r \rightarrow R^+} V_e^{T,\bar{\rho}^T}(r, \Omega) - V_e^{T,\bar{\rho}^T}(r_i, \Omega) &= 4\pi G \bar{\rho}^T R^2 \sum_{n=0}^{\infty} \frac{1}{2n+1} \left[1 - \left(1 + \frac{H}{R} \right)^{-n-1} \right] \\ &\times \sum_{k=0}^{n+2} \binom{n+2}{k} \frac{1}{R^{k+1}} \frac{1}{k+1} \sum_{m=-n}^n H_{n,m}^{(k+1)} Y_{n,m}(\Omega). \end{aligned} \tag{37}$$

Sjöberg (2007) derived the topographic bias in the following form

$$\lim_{r \rightarrow R^+} V_e^{T,\bar{\rho}^T}(r, \Omega) - \lim_{r \rightarrow R^-} V_i^{T,\bar{\rho}^T}(r, \Omega) = 2\pi G \bar{\rho}^T \left(H^2 + \frac{2}{3R} H^3 \right). \tag{38}$$

The topographic bias represents the discontinuity of the gravitational potential generated by the spherical Bouguer shell at its lower topographic bound, $r = R$. The topographic bias of the spherical roughness term equals zero, because its values evaluated for $r \rightarrow R^+$ and $r \rightarrow R^-$ are the same and thus cancel each other (cf. Sjöberg 2007). With reference to the definition of the (higher-order) Laplace harmonics $\{H_n^{(k)} : k = 2, 3, \dots\}$ of topographic heights in Eq. (9.A), the topographic bias in Eq. (39) is defined in the following spectral form

$$\lim_{r \rightarrow R^+} V_e^{T,\bar{\rho}^T}(r, \Omega) - \lim_{r \rightarrow R^-} V_i^{T,\bar{\rho}^T}(r, \Omega) = 2\pi G \bar{\rho}^T \sum_{n=0}^{\infty} \sum_{m=-n}^n \left(H_{n,m}^{(2)} + \frac{2}{3R} H_{n,m}^{(3)} \right) Y_{n,m}(\Omega). \tag{39}$$

Inserting from Eqs. (37) and (39) to Eq. (34), the spectral expression for the topographic potential difference becomes

$$\begin{aligned} V^{T,\bar{\rho}^T}(r, \Omega) - V^{T,\bar{\rho}^T}(r_i, \Omega) &= 4\pi G \bar{\rho}^T R^2 \sum_{n=0}^{\infty} \frac{1}{2n+1} \left[1 - \left(1 + \frac{H}{R} \right)^{-n-1} \right] \\ &\times \sum_{k=0}^{n+2} \binom{n+2}{k} \frac{1}{R^{k+1}} \frac{1}{k+1} \sum_{m=-n}^n H_{n,m}^{(k+1)} Y_{n,m}(\Omega) \\ &- 2\pi G \bar{\rho}^T \sum_{n=0}^{\infty} \sum_{m=-n}^n \left[H_{n,m}^{(2)} + \frac{2}{3R} H_{n,m}^{(3)} \right] Y_{n,m}(\Omega). \end{aligned} \tag{40}$$

To relate the Laplace harmonics of H_n (and their higher-order terms) with the spherical harmonics which describe the Earth’s gravity field, the constituents on the right-hand side of Eq. (40) are scaled by GM. In the spherical approximation, the geocentric gravitational constant GM is given by

$$GM = \frac{4\pi}{3} GR^3 \bar{\rho}^{\text{Earth}}, \tag{41}$$

where $\bar{\rho}^{\text{Earth}} = 5500 \text{ kg m}^{-3}$ is the Earth’s mean mass density. Combining Eqs. (40) and (41) and limiting the series expansion up to the finite degree of \bar{n} , we get

$$\begin{aligned} V^{T,\bar{\rho}^T}(r_{\text{mg}}, \Omega) - V^{T,\bar{\rho}^T}(r_i, \Omega) &= \frac{GM}{R} \sum_{n=0}^{\bar{n}} \left[1 - \left(1 + \frac{H}{R} \right)^{-n-1} \right] \sum_{m=-n}^n V_{n,m}^{T,\bar{\rho}^T} Y_{n,m}(\Omega) \\ &- \frac{GM}{R} \sum_{n=0}^{\bar{n}} \sum_{m=-n}^n V_{n,m}^{\text{bias}} Y_{n,m}(\Omega), \end{aligned} \tag{42}$$

where the potential coefficients $V_{n,m}^{T,\bar{\rho}^T}$ read

$$V_{n,m}^{T,\bar{\rho}^T} = \frac{3}{2n+1} \frac{\bar{\rho}^T}{\bar{\rho}^{\text{Earth}}} \sum_{k=0}^{n+2} \binom{n+2}{k} \frac{1}{k+1} \frac{H_{n,m}^{(k+1)}}{R^{k+1}}, \tag{43}$$

and the topographic bias coefficients $V_{n,m}^{\text{bias}}$ are given by

$$V_{n,m}^{\text{bias}} = 3 \frac{\bar{\rho}^T}{\bar{\rho}^{\text{Earth}}} \sum_{k=1}^2 \frac{1}{k+1} \frac{H_{n,m}^{(k+1)}}{R^{k+1}}. \tag{44}$$

As seen in Eqs. (43) and (44), the potential coefficients $V_{n,m}^{T,\bar{\rho}^T}$ comprise the first- and higher-order terms of the Laplace harmonics of topographic heights (up to a chosen maximum degree of the spectral resolution used for the computation), while the topographic bias coefficients $V_{n,m}^{\text{bias}}$ comprise only the second- and third-order Laplace harmonics. This is because the terrain roughness term in the definition of the topographic bias is absent.

4.2 Topographic Potential Difference (of Anomalous Density)

The topographic potential $V^{T,\delta\rho^T}$ generated by the anomalous topographic density distribution can be defined in terms of the Laplace harmonics of $\delta\rho^T H_n$ and their higher-order terms $\{\delta\rho^T H_n^{(k)} : k = 2, 3, \dots\}$ if the density function $\delta\rho^T$ describes uniquely the anomalous density distribution within the whole topography. This is possible only if the radial density distribution is continuous everywhere within the topography. In reality, however, the density distribution within the upper continental crust comprises density contrast interfaces, such as below the polar ice sheets or sedimentary basins and the underlying bedrock. For this reason, we separate the anomalous topographic density into particular continental crustal components (within the topography) attributed to the continental water bodies (lakes), ice, sediments and remaining anomalous topographic masses. This description utilizes the volumetric mass layer of a particular density structure enclosed by the upper and lower bounds of this volumetric layer. The geometry of the upper and lower bounds is defined by their heights H_U and H_L relative to the geoid surface (which is approximated by the radius R). In the most general case, the actual density ρ within every volumetric mass layer can be approximated by the laterally distributed radial density variation model using the following polynomial function (Tenzer et al. 2012a)

$$\rho(r, \Omega) = \rho(H_U, \Omega) + \beta(\Omega) \sum_{i=1}^I \alpha_i(\Omega) (r - R)^i, \tag{45}$$

for $R + H_U(\Omega) \geq r > R + H_L(\Omega)$,

where $\rho(H_U, \Omega)$ is the (nominal) lateral density stipulated at the upper bound H_U and a location Ω . The radial density change with respect to the nominal density $\rho(H_U, \Omega)$ is described by the parameters β and $\{\alpha_i : i = 1, 2, \dots, I\}$, where I is the maximum order of the radial density distribution function.

Since the anomalous topographic density $\delta\rho^T$ is defined with respect to the reference topographic density $\bar{\rho}^T$, we further define the density contrast within a volumetric mass layer by

$$\begin{aligned}\delta\rho(r, \Omega) &= \rho(r, \Omega) - \bar{\rho}^T \\ &= \delta\rho(H_U, \Omega) + \beta(\Omega) \sum_{i=1}^I \alpha_i(\Omega)(r - R)^i, \\ &\text{for } R + H_U(\Omega) \geq r > R + H_L(\Omega),\end{aligned}\quad (46)$$

where $\delta\rho(H_U, \Omega)$ is the nominal value of the lateral density contrast at (H_U, Ω) .

In Sect. 4.1, we derived the topographic potential difference (of reference density) $\lim_{r \rightarrow R^-} V_i^{T, \bar{\rho}^T}(r, \Omega) - V_e^{T, \bar{\rho}^T}(r_t, \Omega)$ by means of the analytical continuation term and the topographic bias (see Eq. 42), because the analytical downward continuation of the topographic potential was in this case permissible. For the anomalous topographic density distribution, however, this mathematical formalism is not applicable, due to presence of mass density discontinuities. For this reason, we define the gravitational potential difference of a volumetric mass density contrast layer in terms of the potentials for the internal and external convergence domains, i.e. $V^{\delta\rho^T}(r_g, \Omega) - V^{\delta\rho^T}(r_t, \Omega) = \lim_{r \rightarrow R^-} V_i^{\delta\rho}(r, \Omega) - V_e^{\delta\rho}(r_t, \Omega)$. The gravitational potentials (of anomalous mass density contrast layer) for the external and internal convergence domains are derived in Appendices 2 and 3, respectively.

With reference to Eqs. (71) and (84), the potential difference of a volumetric mass density contrast layer is obtained in the following form

$$\lim_{r \rightarrow R^-} V_i^{\delta\rho}(r, \Omega) - V_e^{\delta\rho}(r_t, \Omega) = \frac{GM}{R} \sum_{n=0}^{\bar{n}} \sum_{m=-n}^n \left[iV_{n,m}^{\delta\rho} - \left(\frac{R}{R+H} \right)^{n+1} eV_{n,m}^{\delta\rho} \right] Y_{n,m}(\Omega), \quad (47)$$

where the potential coefficients $eV_{n,m}^{\delta\rho}$ and $iV_{n,m}^{\delta\rho}$ for the external and internal convergence domains are defined in Eqs. (72) and (85), respectively. Since the anomalous density distribution within the whole topography is generally described by several individual volumetric mass layers, the gravitational effect of anomalous topographic density is defined as a sum of the potentials generated by these layers.

4.3 No-Topography Disturbing Potential Difference

To evaluate the non-topographic part of the disturbing potential difference in Eq. (14), we first subtract the topographic potential V^T from the disturbing potential T , both referred at the topographic surface. The disturbing potential T at the topographic surface (r_t, Ω) reads (e.g., Heiskanen and Moritz 1967, Chap 2–14)

$$T(r_t, \Omega) = \frac{GM}{R} \sum_{n=0}^{\bar{n}} \sum_{m=-n}^n \left(\frac{R}{r_t} \right)^{n+1} T_{n,m} Y_{n,m}(\Omega), \quad (48)$$

where $T_{n,m}$ are the (fully normalized) numerical coefficients which describe the disturbing potential T . The coefficients $T_{n,m}$ are obtained from the coefficients of a global gravitational model after subtracting the spherical harmonic coefficients of the GRS80 normal gravity field (Moritz 2000).

By analogy with Eq. (48), we define the no-topography disturbing potential T^{NT} at the topographic surface (r_t, Ω) by subtracting the topographic potential V^T from T . With reference to the decomposition of the topographic potential in Eq. (13), we write

$$T^{NT}(r_t, \Omega) = T(r_t, \Omega) - V_e^{T, \bar{\rho}^T}(r_t, \Omega) - \sum_j V_{ej}^{\delta\rho}(r_t, \Omega), \quad (49)$$

where j is the summation index of the volumetric mass density contrast layers applied to describe the anomalous density distribution within the whole topography. The corresponding spectral representation of the no-topography disturbing potential T^{NT} at the topographic surface reads

$$T^{NT}(r_t, \Omega) = \frac{GM}{R} \sum_{n=0}^{\bar{n}} \sum_{m=-n}^n \left(\frac{R}{r_t}\right)^{n+1} \left(T_{n,m} - V_{n,m}^{T, \bar{\rho}^T} - \sum_j e V_{n,mj}^{\delta\rho} \right) Y_{n,m}(\Omega). \quad (50)$$

The computation of the no-topography gravity field quantities according to Eq (50) is realized by generating spherical harmonic coefficients of the no-topography disturbing potential, i.e. $T_{n,m}^{NT} = T_{n,m} - V_{n,m}^{T, \bar{\rho}^T} - \sum_j e V_{n,mj}^{\delta\rho}$. These coefficients are then used to compute the no-topography disturbing potential difference from

$$T^{NT}(r_g, \Omega) - T^{NT}(r_t, \Omega) = \frac{GM}{R} \sum_{n=0}^{\bar{n}} \sum_{m=-n}^n \left[1 - \left(1 + \frac{H}{R}\right)^{-n-1} \right] T_{n,m}^{NT} Y_{n,m}(\Omega). \quad (51)$$

4.4 Normal Gravity Difference Term

The expression for the geoid-to-quasigeoid correction in Eq. (11a) comprises also the normal gravity difference term. For consistency, this term should be computed with the same spectral resolution as the disturbing potential difference term using the following expression

$$\frac{2}{R} H(\Omega) \zeta(\Omega) = \frac{2}{R} \sum_{n=0}^{\bar{n}} \sum_{m=-n}^n H_{n,m} Y_{n,m}(\Omega) \sum_{n=0}^{\bar{n}} \sum_{m=-n}^n \varsigma_{n,m} Y_{n,m}(\Omega). \quad (52)$$

The height anomaly coefficients $\varsigma_{n,m}$ in Eq. (52) are generated from the disturbing potential coefficients $T_{n,m}$ (scaled by the factor γ^{-1}). Hence

$$\varsigma_{n,m} = \frac{T_{n,m}}{\gamma(H^N, \phi)}. \quad (53)$$

5 Discussion

The geoid-to-quasigeoid correction is often computed only approximately as a function of the simple planar Bouguer gravity anomaly and the topographic height for a conversion between Molodensky's normal and Helmert's orthometric heights. For practical reasons, this simple formula would preferably be used for most applications. Moreover, it provides a relatively good accuracy over flat regions. In mountainous, polar and geologically complex regions, however, the errors in computed values of the geoid-to-quasigeoid correction can reach up to several decimetres (e.g., Santos et al. 2006). To reduce these errors to reach the centimetre level accuracy, the computation should be done more accurately using the expression derived in Eq. (11).

The numerical procedures developed in this study incorporate terrain and crustal density models in the definition of the geoid-to-quasigeoid correction while also taking the effect of mass density heterogeneities distributed below the geoid surface into consideration. As already emphasized, the application of more accurate methods is needed especially in the mountainous regions. This was demonstrated, for instance, by Sjöberg and Bagherbandi (2012) who estimated, based on using the EGM2008 coefficients (Pavlis et al. 2012) complete to a spherical harmonic degree of 2160, that the geoid-to-quasigeoid correction reaches a maximum of ~ 5.5 m in the Himalayas. Bagherbandi and Tenzer (2013) used the GOCO02S coefficients (Goinger et al. 2011) up to degree/order 250 to estimate this correction in central Eurasia. According to their result this correction reaches a maximum of ~ 3.6 m in the Himalayas. They applied the method of Sjöberg (2010) which takes the effects of terrain and lateral topographic density into consideration. Although the effect of variable topographic density was disregarded in these numerical studies, the terrain geometry alone changed the value of the geoid-to-quasigeoid correction considerably. The differences between the maximum values of the geoid-to-quasigeoid correction in the Himalayas estimated by Sjöberg and Bagherbandi (2012) and Bagherbandi and Tenzer (2013) are explained by the fact that this correction is very sensitive on the maximum degree of spherical harmonics used for the computation. These two estimates also differ significantly from the maximum value of this correction in the Himalayas of only ~ 2 m when computed as a function of the simple planar Bouguer gravity anomaly and the topographic height (e.g., Rapp 1997). The effect of terrain geometry on the geoid-to-quasigeoid correction is thus significant. Nevertheless, all these values were estimated according to computational models which take only topography into consideration while disregarding the effect of mass density heterogeneities distributed below the geoid surface. The assumption that the geoid-to-quasigeoid correction could not be computed accurately without taking the non-topographic effect into consideration was confirmed by Tenzer et al. (2005). They demonstrated, based on the numerical results in a high-elevation and rugged part of the Canadian Rocky Mountains, that the effect of topographic density variations varies from -7 to 2 cm, while the total topographic effect (including the variable topographic density) on the geoid-to-quasigeoid correction is between -86.5 and 0.1 cm. In contrast, they estimated that the non-topographic effect is mostly positive and varies within a range of -8 to 44 cm. Since the non-topographic effect is mostly of opposite sign than the topographic effect, the combined effect to the geoid-to-quasigeoid correction cancels to some extent, especially at the long-to-medium wavelengths where isostatic compensation prevails. According to their results the geoid-to-quasigeoid correction is everywhere negative and varies from -0.1 to -45.6 cm which is only about a half of the total topographic effect. These results also revealed that the gravitational contribution of mass density heterogeneities distributed below the geoid surface is actually much larger than the effect of variable topographic density. Based on these results, we argue that the estimation of the non-topographic effect to the geoid-to-quasigeoid correction is essential especially in the mountainous regions due to the presence of isostatic compensation. This isostatic effect could be attributed to either variable crustal density (i.e. Pratt's (1855) isostatic principle) or variable crustal thickness (i.e. Airy's (1855) isostatic principle). In reality, however, both these isostatic models represent only extreme cases, while the actual crustal mass balance is much more complex and involving also geodynamic processes (such as active tectonism, postglacial rebound, crustal flexure, mantle viscoelasticity). Nevertheless, in mountainous areas the isostasy typically more closely

agrees with Airy's model, while Pratt's model better approximates the isostasy over oceans.

The effect of variable topographic density on the geoid-to-quasigeoid correction could in some regions be also very significant. A typical example can be given for polar regions of Antarctica and Greenland with thick coverings of continental ice sheets (reaching up to ~ 4 km at places). In this case, the knowledge of the bedrock topography is essential to determine the depth to which the density of ice should be used instead of the rock density. When disregarding lakes and polar ice sheets, the topographic density still varies over a relatively large interval. Martinec (1998), for instance, mentioned that the topographic density variations worldwide are typically within ± 300 kg m⁻³ around the average value of 2670 kg m⁻³. These density variations correspond to changes in the geoid-to-quasigeoid correction to ~ 10 % (cf. Huang et al. 2001). Even larger topographic mass density variations (~ 20 – 30 %) are encountered in some other parts of the world (e.g., Tziavos and Featherstone 2001). Tenzer et al. (2011c), for instance, inferred the density variations of main rock types in New Zealand between 900 kg m⁻³ (Loess) and 3300 kg m⁻³ (Dunite) based on the analysis of in situ density measurements and digital geological maps. These large topographic density variations could cause changes in the geoid-to-quasigeoid corrections up to several decimetres (Vaníček et al. 1995; Allister and Featherstone 2001; Tenzer and Vaníček 2003; Hwang and Hsiao 2003).

The computation of the geoid-to-quasigeoid correction in regional applications is commonly realized in the spatial domain from detailed gravity, terrain and crustal density data. Given that the gravitational signature of deep mantle density heterogeneities has a prevailing long-wavelength pattern, the effect of distant zones should also be taken into consideration. By analogy with the gravimetric geoid/quasigeoid determination, the computation of this correction can then be realized separately for the reference and residual components by applying the remove-compute-restore numerical scheme. Following this principle, the spectral expressions developed in Sect. 4 can be used to compute the (long-to-medium wavelength) reference part of this correction. Subsequently, the (higher-frequency) residual part can be computed from more detailed regional datasets according to the numerical procedures provided in Sect. 3. Although this scheme has been routinely used for the gravimetric geoid/quasigeoid modelling, it has not yet been applied for computing this correction. The main reason is probably that the classical definitions assume that most of the differences between the geoid and the quasigeoid are attributed to the terrain geometry and the topographic density distribution in proximity of the computation point. Tenzer et al. (2005), however, demonstrated that the non-topographic effect on the geoid-to-quasigeoid correction can be significant. Since they used only the regional data while disregarding the gravitational contribution of distant masses, we expect that the non-topographic effect could reach even larger values than those estimated in their study. This aspect has yet to be confirmed numerically. Nevertheless, it is clear that the practical computation of this correction even for regional applications would probably require numerically complex procedures, very similar to those used for the gravimetric geoid/quasigeoid determination.

In Sect. 3, we presented newly developed numerical procedures for computing the geoid-to-quasigeoid correction from discrete gravity disturbances/anomalies. This procedure comprises four individual numerical steps (Fig. 2a, b). By analogy with the gravimetric geoid determination, the gravitational effect of topographic masses is subtracted from the observed gravity data (the first step) and then added back to the resulting (no-topography) disturbing potential difference (the fourth step). The computation of the non-topographic contribution utilizes the gravity-to-potential conversion based on solving

inverse to discretized Green's integral equation (the second step) with the subsequent upward continuation of the no-topography disturbing potential from the geoid to the topographic surface (the third step). Tenzer and Novák (2008) investigated the conditionality of inverse solutions to discretized integral equations in geoid modelling from local gravity data. They demonstrated that the downward continuation procedure by means of solving the inverse to discretized Green's integral equations (Eqs. 21 and 22) is numerically more stable than Poisson's downward continuation (Eqs. 27 and 30). The gravity-to-potential conversion proposed in this study is thus more suitable than the gravity downward continuation used in the previous studies by Tenzer et al. (2005, 2006) and Sjöberg (2006), because it recovers a smoother potential field (at the geoid) from the more detailed gravity field (at the topographic surface). By way of contrast, the recovery of the more detailed gravity field (at the geoid) is required from a smoother gravity field (at the topographic surface) in the gravity downward continuation.

Since currently available detailed gravity datasets around the world are provided to users in the form of either the gravity anomalies or the gravity disturbances, the newly developed numerical procedures in Sect. 3 were derived for both these gravity data types. As seen in Eqs. (21) and (22), the Green integral kernel for the no-topography gravity disturbances is defined as the negative of the Poisson's kernel $-\partial P/\partial r$, while the Green integral kernel for the corresponding gravity disturbance comprises an additional term $2P/r$. Regarding the existing methods, Tenzer et al. (2005) formulated this problem for the no-topography gravity disturbances (see Fig. 2c). According to their approach, the gravity disturbances are first downward continued to the geoid by solving the inverse to discretized Poisson's equation (Eq. 27). These downward-continued gravity disturbances are then used to compute the integral mean of the (no-topography) gravity disturbances (Eq. 29). The conversion between the gravity and potential is in this case avoided. In the alternative method by Tenzer et al. (2006) and Sjöberg (2006), they modified this problem for the gravity anomalies. The (no-topography) gravity anomalies are again downward continued on the geoid by solving the inverse to discretized Poisson's equation (Eq. 30). Subsequently, they solve the generalized Stokes's problem (Eq. 31) for computing the (no-topography) disturbing potential difference from the respective gravity anomalies at the geoid (see Fig. 2d). This type of input gravity data also has implications on the applied topographic correction. As seen in Eqs. (15) and (16), the direct topographic effect is subtracted from the observed gravity disturbances, while the secondary indirect topographic effects have to be taken also into consideration when using the gravity anomalies. The reasons were explained by Vaníček et al. (2005).

The principal difference between the computation of the geoid-to-quasigeoid correction in the spatial and spectral domains is that in the former the gravity data are either converted to the potential values or used directly to compute the potential difference by means of the integral mean of gravity (Sect. 3). In the latter, the computation of the geoid-to-quasigeoid correction is realized by means of the potential field (Sect. 4). The gravity-to-potential conversion is thus not required. This is possible because the EGM coefficients can directly be used to compute the disturbing potential. Similarly, the topographic and crustal density models can directly be used to compute the topographic potential. The disturbing potential difference is then computed individually for the no-topography disturbing potential difference and the topographic potential difference. Moreover, the topographic potential is treated separately for the reference and anomalous topographic density distributions. Compared to existing spectral expressions (e.g., Sjöberg 2010), this newly developed spectral procedure allows modelling of the anomalous topographic density distribution using a 3D density contrast model (Eq. 46). The anomalous density distribution within the

whole topography is approximated by a finite number of volumetric mass layers of which density is described by the laterally distributed radial density variation model. These layers are used to represent major known crustal density structures. The uniform density contrast model is, for example, suitable to approximate the density contrast of continental ice sheets and continental water bodies (lakes). The lateral density model (of multiple layers) can be implemented to describe the density contrast structures within the sediments and remaining upper continental crust. Alternatively, the increasing density with depth within sedimentary basins due to compaction can be described more realistically by assuming a depth-dependent density model (e.g., Artemjev et al. 1994) or—in the most general case—by a 3D density model if information on lateral density structure within sedimentary basins is also known. The most significant improvement in the proposed method is the computation of the non-topographic effect in terms of the no-topography disturbing potential difference. In this way, the change of gravity within the topography attributed to mass density distribution below the geoid surface is taken into consideration, while the spectral expressions in published studies do not account for these gravity variations. As already stated, this effect is significant and cannot be neglected.

6 Summary and Concluding Remarks

Since Molodensky's concept does not require any hypothesis on the density distribution within the topography, normal heights can be computed with the accuracy which is limited only by cumulative and random errors in geodetic spirit levelling and gravity measurements along levelling lines. Molodensky's concept also has some practical advantages related to the definition of the height anomaly for the external gravity field (i.e. the definition of the disturbing potential at the topographic surface), which can be facilitated, for instance, in testing the accuracy of global geopotential models and for the estimation of local vertical datum (LVD) offsets using the Global Navigation Satellite System (GNSS) and levelling data (e.g., Burke et al. 1996; Burša et al. 1997, 1999, 2001; Grafarend and Ardalan 1997; Ardalan and Grafarend 1999). Compared to Molodensky's concept, Helmert's orthometric heights approximate more closely the actual length of the plumbline between the topographic surface and the geoid. This is possible because the Poincaré–Prey gravity gradient in Helmert's definition of mean gravity satisfies Poisson's equation inside the topography, whereas the normal gravity gradient in Molodensky's definition does not (it assumes no masses above the reference ellipsoid). In Helmert's definition, however, only a uniform topographic density model is assumed, disregarding the effects of terrain, variable topographic density and mass density distribution below the geoid surface (i.e. the non-topographic effect). In Niethammer and Mader's definitions, the gravity gradient within the topography is computed more realistically by incorporating the planar terrain correction into Poincaré–Prey's gravity gradient (see also Santos et al. 2006). In more recent studies, not only the terrain effect, but eventually also the anomalous topographic density distribution was taken into consideration in theoretical derivations and practical computations (e.g., Tenzer and Vaníček 2003; Flury and Rummel 2009; Sjöberg 2010, 2012). The most comprehensive methods of computing the geoid-to-quasigeoid correction and orthometric heights by taking the non-topographic effect into consideration were presented in studies by Tenzer (2004), Sjöberg (2006), Tenzer et al. (2005, 2006) and Santos et al. (2006).

In this study, we developed numerical procedures for computing the non-topographic effect on the geoid-to-quasigeoid correction by means of applying the inverse solutions to discretized Green's integral equations. A theoretical foundation of this numerical scheme was given by Novák (2003), who first applied this method in gravimetric geoid determination. According to these numerical procedures, the no-topography gravity disturbances/anomalies at the topographic surface (and corrected for the topographic effect) are directly converted to the respective disturbing potential values at the geoid surface. As discussed in Sect. 5, the main advantage of the gravity-to-potential conversion is its better numerical stability compared to the gravity downward continuation. The no-topography disturbing potential difference is then computed in the successive numerical steps by solving the discretized Poisson's integral. The gravity-to-potential conversion is thus explicitly incorporated in the downward continuation procedure, while in the previous studies this conversion was realized in the successive steps of the upward continuation procedure (after applying the gravity downward continuation). In particular, Tenzer et al. (2005) applied the inverse solution to the discretized Poisson's integral equation for the downward continuation of the no-topography gravity disturbances. They then solved the integral mean of discretized Poisson's integral for computing the non-topographic part of the disturbing potential difference. In the alternative method of computing the geoid-to-quasigeoid correction from the observed gravity anomalies, Tenzer et al. (2006) and Sjöberg (2006) proposed to apply the inverse solution to discretized Poisson's integral equations for the downward continuation of the no-topography gravity anomalies. They then solved the generalized Stokes's problem to compute the (no-topography) disturbing potential difference from the respective gravity anomalies at the geoid surface. Similarly, Hotine's integrals can be used in this numerical step if gravity disturbances are used instead of gravity anomalies. We note that the application of Hotine's approach in computing the geoid-to-quasigeoid correction is still open for investigation.

Another theoretical development in this study was related to the computation of the geoid-to-quasigeoid correction in the spectral domain. These spectral expressions can be applied to evaluate the long-to-medium wavelength part of the geoid-to-quasigeoid correction in the remove-compute-restore numerical scheme, entirely in spherical harmonics, while the remaining higher-frequency part of this correction could be computed in the spatial domain. In the spectral approach, the computation of the topographic potential difference is realized individually for the reference and anomalous topographic density distributions. By analogy with Sjöberg (2007), we have defined the potential difference of the reference topographic density by means of applying the analytical continuation of topographic potential and the topographic bias. The anomalous density distribution within the topography was described by a finite number of the volumetric mass density contrast layers. The gravitational effect of each volumetric mass density contrast layer on the geoid-to-quasigeoid correction can be computed according to the expressions derived in Tenzer et al. (2012a). These expressions, modified for computing the potential difference of the volumetric mass density contrast layer, were defined in terms of the potential coefficients for the external and internal convergence domains. The non-topographic part of the gravity field is then generated from the spherical harmonic coefficients of the Earth's gravity field after subtracting the topographic potential coefficients.

Acknowledgments This research was supported by the National Program of Sustainability, Project No.: LO1506, Czech Ministry of Education, Youth and Sport.

Appendix 1: Potential (of Reference Topographic Density) for External Convergence Domain

To find the spectral representation of the Newton volumetric integral in Eq. (17) for the external convergence domain, we define the fundamental harmonic function ℓ^{-1} by (e.g., Heiskanen and Moritz 1967, Eqs. 1–81)

$$\ell^{-1}(r, \psi, r') = \frac{1}{r} \sum_{n=0}^{\infty} \left(\frac{r'}{r}\right)^n P_n(t) \quad (r \geq r'), \tag{54}$$

where P_n is the Legendre polynomial of degree n , and $t = \cos \psi$. Inserting Eq. (54) in Eq. (17), the topographic potential V_e^{T, ρ^T} for the external convergence domain $r \geq r'$ becomes

$$V_e^{T, \rho^T}(r, \Omega) = G \bar{\rho}^T r \sum_{n=0}^{\infty} \iint_{\phi} P_n(t) \int_{r'=R}^{R+H'} \left(\frac{r'}{r}\right)^{n+2} dr' d\Omega'. \tag{55}$$

The radial integral in Eq. (55) is further rearranged into the form

$$\int_{r'=R}^{R+H'} \left(\frac{r'}{r}\right)^{n+2} dr' = \int_{r'=R}^{R+H'} \left(\frac{R}{r}\right)^{n+2} (1 + \eta)^{n+2} dr' \quad (n = 0, 1, \dots), \tag{56}$$

where $\eta = (r' - R)/R$. Applying a binomial theorem to $(1 + \eta)^{n+2}$, we get

$$(1 + \eta)^{n+2} \cong \sum_{k=0}^{n+2} \binom{n+2}{k} \left(\frac{r' - R}{R}\right)^k \quad (n = 0, 1, \dots). \tag{57}$$

Substituting Eq. (57) in Eq. (56) yields

$$\int_{r'=R}^{R+H'} \left(\frac{r'}{r}\right)^{n+2} dr' \cong \int_{r'=R}^{R+H'} \left(\frac{R}{r}\right)^{n+2} \sum_{k=0}^{n+2} \binom{n+2}{k} \left(\frac{r' - R}{R}\right)^k dr' \quad (n = 0, 1, \dots). \tag{58}$$

Solving the radial integral in Eq. (58) and inserting for the integral limits, we arrive at

$$\begin{aligned} \int_{r'=R}^{R+H'} \left(\frac{r'}{r}\right)^{n+2} dr' &\cong \left(\frac{R}{r}\right)^{n+2} \sum_{k=0}^{n+2} \binom{n+2}{k} \frac{1}{R^k} \frac{(r' - R)^{k+1}}{k+1} \Big|_{r'=R}^{R+H'} \\ &= R \left(\frac{R}{r}\right)^{n+2} \sum_{k=0}^{n+2} \binom{n+2}{k} \left(\frac{H'}{R}\right)^{k+1} \frac{1}{k+1} \quad (n = 0, 1, \dots), \end{aligned} \tag{59}$$

where $H' = r' - R$. Substituting Eq. (59) in Eq. (55), the spectral form of V_e^{T, ρ^T} becomes

$$\begin{aligned} V_e^{T, \rho^T}(r, \Omega) &\cong G \bar{\rho}^T R^2 \sum_{n=0}^{\infty} \left(\frac{R}{r}\right)^{n+1} \\ &\quad \times \sum_{k=0}^{n+2} \binom{n+2}{k} \frac{1}{R^{k+1}} \frac{1}{k+1} \iint_{\phi} H'^{k+1} P_n(t) d\Omega' \end{aligned} \tag{60}$$

Since the expansion of V_e^{T, ρ^T} into a series of spherical functions converges uniformly for the external convergence domain $r \geq R$, the interchange of summation and integration in

Eq. (60) was permitted (cf. Moritz 1990). We note here that the same spectral form of Newton's integral for the external convergence domain as derived in Eq. (61) can be found by changing the order of applying the radial integration and binomial theorem (cf. Årgen 2004; Vermeer 2008).

The Laplace harmonics H_n of the topographic heights in Eq. (61) are defined by the following integral convolution

$$H(\Omega) = \sum_{n=0}^{\infty} H_n(\Omega), H_n(\Omega) = \frac{2n+1}{4\pi} \iint_{\phi} H' P_n(t) d\Omega' = \sum_{m=-n}^n H_{n,m} Y_{n,m}(\Omega), \quad (61)$$

where $H_{n,m}$ are the topographic height coefficients. The corresponding higher-order harmonics $\{H_n^{(k)} : k = 2, 3, \dots\}$ read

$$\begin{aligned} H_n^{(k)}(\Omega) &= \frac{2n+1}{4\pi} \iint_{\phi} H'^k P_n(t) d\Omega' \\ &= \sum_{m=-n}^n H_{n,m}^{(k)} Y_{n,m}(\Omega). \end{aligned} \quad (62)$$

Substituting Eqs. (61) and (62) in Eq. (60), the topographic potential $V_e^{T,\bar{\rho}^T}$ is obtained in the following spectral form

$$\begin{aligned} V_e^{T,\bar{\rho}^T}(r, \Omega) &= 4\pi G \bar{\rho}^T R^2 \sum_{n=0}^{\infty} \left(\frac{R}{r}\right)^{n+1} \frac{1}{2n+1} \\ &\times \sum_{k=0}^{n+2} \binom{n+2}{k} \frac{1}{R^{k+1}} \frac{1}{k+1} \sum_{m=-n}^n H_{n,m}^{(k+1)} Y_{n,m}(\Omega). \end{aligned} \quad (63)$$

Appendix 2: Potential (of Anomalous Mass Density Contrast Layer) for External Convergence Domain

To find the spectral expression of the gravitational potential $V_e^{\delta\rho}$ (of anomalous mass density contrast layer) for the external convergence domain, we first substitute the density contrast model from Eq. (46) to Newton's integral in Eq. (18). After limiting the integration domain to the volumetric mass layer, the gravitational potential $V^{\delta\rho}$ becomes

$$\begin{aligned} V^{\delta\rho}(r, \Omega) &\cong G \iint_{\phi} \delta\rho(H'_U, \Omega') \int_{r'=R+H'_L}^{R+H'_U} \ell^{-1}(r, \psi, r') r'^2 dr' d\Omega' \\ &+ G \iint_{\phi} \int_{r'=R+H'_L}^{R+H'_U} \beta(\Omega') \sum_{i=1}^I \alpha_i(\Omega') (r' - R)^i \ell^{-1}(r, \psi, r') r'^2 dr' d\Omega'. \end{aligned} \quad (64)$$

We note that the parameters H_U, H_L and $\rho(H_U, \Omega)$ become H'_U, H'_L and $\rho(H'_U, \Omega')$ when used for volumetric integration on the right-hand side of Eq. (64), because the position of integration point is described by the coordinates (r', Ω') .

We further define the spectral form of $V_e^{\delta\rho}$ in Eq. (64) for the external convergence domain. Inserting from Eq. (54) to Eq. (64), we get

$$\begin{aligned}
 V_e^{\delta\rho}(r, \Omega) &\cong Gr \sum_{n=0}^{\infty} \iint_{\phi} \delta\rho(H'_U, \Omega') P_n(t) \int_{r'=R+H'_L}^{R+H'_U} \left(\frac{r'}{r}\right)^{n+2} dr' d\Omega' \\
 &\quad + Gr \sum_{n=0}^{\infty} \iint_{\phi} \beta(\Omega') \sum_{i=1}^I \alpha_i(\Omega') P_n(t) \int_{r'=R+H'_L}^{R+H'_U} (r' - R)^i \left(\frac{r'}{r}\right)^{n+2} dr' d\Omega'. \quad (65)
 \end{aligned}$$

The solution of the radial integral in the first constituent on the right-hand side of Eq. (65) yields

$$\begin{aligned}
 \int_{r'=R+H'_L}^{R+H'_U} \left(\frac{r'}{r}\right)^{n+2} dr' &= \left(\frac{R}{r}\right)^{n+2} \int_{r'=R+H'_L}^{R+H'_U} \left(1 + \frac{r' - R}{R}\right)^{n+2} dr' \\
 &\cong \left(\frac{R}{r}\right)^{n+2} \int_{r'=R+H'_L}^{R+H'_U} \sum_{k=0}^{n+2} \binom{n+2}{k} \left(\frac{r' - R}{R}\right)^k dr' \\
 &= \left(\frac{R}{r}\right)^{n+2} \sum_{k=0}^{n+2} \binom{n+2}{k} \frac{1}{R^k} \frac{(r' - R)^{k+1}}{k+1} \Bigg|_{r'=R+H'_L}^{R+H'_U} \\
 &= \left(\frac{R}{r}\right)^{n+2} \sum_{k=0}^{n+2} \binom{n+2}{k} \frac{1}{R^k} \frac{H_U^{k+1} - H'_L^{k+1}}{k+1} \quad (n = 0, 1, \dots). \quad (66)
 \end{aligned}$$

Similarly, the solution of the radial integral in the second constituent on the right-hand side of Eq. (65) is found to be

$$\begin{aligned}
 \int_{r'=R+H'_L}^{R+H'_U} (r' - R)^i \left(\frac{r'}{r}\right)^{n+2} dr' &= \left(\frac{R}{r}\right)^{n+2} \int_{r'=R+H'_L}^{R+H'_U} (r' - R)^i \left(1 + \frac{r' - R}{R}\right)^{n+2} dr' \\
 &\cong \left(\frac{R}{r}\right)^{n+2} \int_{r'=R+H'_L}^{R+H'_U} \sum_{k=0}^{n+2} \binom{n+2}{k} \frac{(r' - R)^{k+i}}{R^k} dr' \\
 &= \left(\frac{R}{r}\right)^{n+2} \sum_{k=0}^{n+2} \binom{n+2}{k} \frac{1}{R^k} \frac{H_U^{k+i+1} - H'_L^{k+i+1}}{k+1+i} \quad (n = 0, 1, \dots; i = 1, 2, \dots, I). \quad (67)
 \end{aligned}$$

Inserting from Eqs. (66) and (67) to Eq. (65), we get

$$\begin{aligned}
 V_e^{\delta\rho}(r, \Omega) &\cong GR \sum_{n=0}^{\infty} \left(\frac{R}{r}\right)^{n+1} \sum_{k=0}^{n+2} \binom{n+2}{k} \frac{1}{R^k} \frac{1}{k+1} \\
 &\quad \times \iint_{\phi} \delta\rho(H'_U, \Omega') (H_U^{k+i+1} - H'_L^{k+i+1}) P_n(t) d\Omega' \\
 &\quad + GR \sum_{n=0}^{\infty} \left(\frac{R}{r}\right)^{n+1} \sum_{i=1}^I \sum_{k=0}^{n+2} \binom{n+2}{k} \frac{1}{R^k} \frac{1}{k+1+i} \\
 &\quad \times \iint_{\phi} \beta(\Omega') \alpha_i(\Omega') (H_U^{k+i+1} - H'_L^{k+i+1}) P_n(t) d\Omega'. \quad (68)
 \end{aligned}$$

Tenzer et al. (2012a, b) defined the spherical lower-bound and upper-bound functions L_n and U_n of a volumetric mass density contrast layer and their higher-order terms in the following form

$$L_n^{(k+1+i)}(\Omega) = \begin{cases} \frac{2n+1}{4\pi} \iint_{\phi} \delta\rho(H'_U, \dot{\Omega}') H_L^{k+1}(\Omega') P_n(t) d\Omega' \\ = \sum_{m=-n}^n L_{n,m}^{(k+1)} Y_{n,m}(\Omega) & i = 0 \\ \frac{2n+1}{4\pi} \iint_{\phi} \beta(\Omega') \alpha_i(\Omega') H_L^{k+1+i}(\Omega') P_n(t) d\Omega' \\ = \sum_{m=-n}^n L_{n,m}^{(k+1+i)} Y_{n,m}(\Omega) & i = 1, 2, \dots, I \end{cases} \tag{69}$$

and

$$U_n^{(k+1+i)}(\Omega) = \begin{cases} \frac{2n+1}{4\pi} \iint_{\phi} \delta\rho(H'_U, \Omega') H_U^{k+1}(\Omega') P_n(t) d\Omega' \\ = \sum_{m=-n}^n U_{n,m}^{(k+1)} Y_{n,m}(\Omega) & i = 0 \\ \frac{2n+1}{4\pi} \iint_{\phi} \beta(\Omega') \alpha_i(\Omega') H_U^{k+1+i}(\Omega') P_n(t) d\Omega' \\ = \sum_{m=-n}^n U_{n,m}^{(k+1+i)} Y_{n,m}(\Omega) & i = 1, 2, \dots, I \end{cases} \tag{70}$$

Substituting Eqs. (69) and (70) in Eq. (68) and considering the series expansion up to the maximum degree of \bar{n} , we arrive at

$$V_e^{\delta\rho}(r, \Omega) = \frac{GM}{R} \sum_{n=0}^{\bar{n}} \left(\frac{R}{r}\right)^{n+1} \sum_{m=-n}^n eV_{n,m}^{\delta\rho} Y_{n,m}(\Omega), \tag{71}$$

where the potential coefficients $eV_{n,m}^{\delta\rho}$ read

$$eV_{n,m}^{\delta\rho} = \frac{3}{2n+1} \frac{1}{\bar{\rho}_{\text{Earth}}} \sum_{i=0}^I (eFu_{n,m}^{(i)} - eFl_{n,m}^{(i)}). \tag{72}$$

The numerical coefficients $\{ eFl_{n,m}^{(i)}, eFu_{n,m}^{(i)} : i = 0, 1, \dots, I \}$ in Eq. (65) are given by

$$eFl_{n,m}^{(i)} = \sum_{k=0}^{n+2} \binom{n+2}{k} \frac{1}{k+1+i} \frac{L_{n,m}^{(k+1+i)}}{R^{k+1}} \quad (i = 0, 1, \dots, I), \tag{73}$$

and

$$eFu_{n,m}^{(i)} = \sum_{k=0}^{n+2} \binom{n+2}{k} \frac{1}{k+1+i} \frac{U_{n,m}^{(k+1+i)}}{R^{k+1}} \quad (i = 0, 1, \dots, I). \tag{74}$$

Appendix 3: Potential (of Anomalous Mass Density Contrast Layer) for Internal Convergence Domain

We apply a similar procedure as used in “Appendix 2” to derive the spectral expression of the potential $V_i^{\delta\rho}$ (of anomalous mass density contrast layer) for the internal convergence domain. For this purpose, we define the fundamental harmonic function ℓ^{-1} in Eq. (54) for the internal convergence domain $r < r'$ as follows

$$\ell^{-1}(r, \psi, r') = \frac{1}{r'} \sum_{n=0}^{\infty} \left(\frac{r}{r'}\right)^n P_n(t) \quad (r < r'). \tag{75}$$

The substitution from Eq. (75) to Eq. (64) yields

$$\begin{aligned} \lim_{r \rightarrow R^-} V_i^{\delta\rho}(r, \Omega) &= GR \sum_{n=0}^{\infty} \iint_{\phi} \delta\rho(H'_U, \Omega') P_n(t) \int_{r'=R+H'_L}^{R+H'_U} \left(\frac{R}{r'}\right)^{n-1} dr' d\Omega' \\ &+ GR \sum_{n=0}^{\infty} \iint_{\phi} \beta(\Omega') \sum_{i=1}^I \alpha_i(\Omega') P_n(t) \int_{r'=R+H'_U}^{R+H'_U} (r' - R)^i \left(\frac{R}{r'}\right)^{n-1} dr' d\Omega'. \end{aligned} \tag{76}$$

We further rearrange the radial integral in the first constituent on the right-hand side of Eq. (76) into the following form

$$\int_{r'=R+H'_L}^{R+H'_U} \left(\frac{R}{r'}\right)^{n-1} dr' = \int_{r'=R+H'_L}^{R+H'_U} \left(\frac{r'}{R}\right)^{1-n} dr' = \int_{r'=R+H'_L}^{R+H'_U} (1 + \eta)^{1-n} dr' \quad (n = 0, 1, \dots), \tag{77}$$

and apply a binomial theorem to $(1 + \eta)^{1-n}$. Hence

$$\begin{aligned} (1 + \eta)^{1-n} &\cong \sum_{k=0}^{\infty} \binom{1-n}{k} \left(\frac{r' - R}{R}\right)^k = \sum_{k=0}^{\infty} (-1)^k \binom{n+k-2}{k} \left(\frac{r' - R}{R}\right)^k \\ (n = 0, 1, \dots). \end{aligned} \tag{78}$$

Inserting from Eq. (78) to Eq. (77), we get

$$\int_{r'=R+H'_L}^{R+H'_U} \left(\frac{R}{r'}\right)^{n-1} dr' \cong \sum_{k=0}^{\infty} (-1)^k \binom{n+k-2}{k} \int_{r'=R+H'_L}^{R+H'_U} \left(\frac{r' - R}{R}\right)^k dr' \quad (n = 0, 1, \dots). \tag{79}$$

The solution of the radial integral in Eq. (79) reads

$$\begin{aligned} \int_{r'=R+H'_L}^{R+H'_U} \left(\frac{R}{r'}\right)^{n-1} dr' &\cong \sum_{k=0}^{\infty} (-1)^k \binom{n+k-2}{k} \frac{1}{R^k} \frac{(r' - R)^{k+1}}{k+1} \Bigg|_{r'=R+H'_L}^{R+H'_U} \\ &= R \sum_{k=0}^{\infty} (-1)^k \binom{n+k-2}{k} \left(\frac{H'_U - H'_L}{R}\right)^{k+1} \frac{1}{k+1} \quad (n = 0, 1, \dots). \end{aligned} \tag{80}$$

By analogy with Eq. (79), we rewrite the radial integral in the second term on the right-hand side of Eq. (76) as follows

$$\int_{r'=R+H'_L}^{R+H'_U} (r' - R)^i \left(\frac{R}{r'}\right)^{n-1} dr' = \int_{r'=R+H'_L}^{R+H'_U} (r' - R)^i (1 + \eta)^{1-n} dr' \tag{81}$$

$(n = 0, 1, \dots; i = 1, 2, \dots, I).$

The substitution for $(1 + \eta)^{1-n}$ from Eq. (78) to Eq. (81) yields

$$\int_{r'=R+H'_L}^{R+H'_U} (r' - R)^i \left(\frac{R}{r'}\right)^{n-1} dr' \cong R^i \sum_{k=0}^{\infty} (-1)^k \binom{n+k-2}{k} \int_{r'=R+H'_L}^{R+H'_U} \left(\frac{r' - R}{R}\right)^{k+i} dr' \tag{82}$$

$(n = 0, 1, \dots; i = 1, 2, \dots, I).$

The solution of the radial integral in Eq. (82) is then found to be

$$\begin{aligned} \int_{r'=R+H'_L}^{R+H'_U} (r' - R)^i \left(\frac{R}{r'}\right)^{n-1} dr' &\cong \sum_{k=0}^{\infty} (-1)^k \binom{n+k-2}{k} \frac{1}{R^k} \frac{(r' - R)^{k+i+1}}{k+1+i} \Bigg|_{r'=R+H'_L}^{R+H'_U} \\ &= R^{i+1} \sum_{k=0}^{\infty} (-1)^k \binom{n+k-2}{k} \left(\frac{H'_U - H'_L}{R}\right)^{k+i+1} \frac{1}{k+1+i} \end{aligned} \tag{83}$$

$(n = 0, 1, \dots; i = 1, 2, \dots, I).$

Substituting from Eqs. (80) and (83) to Eq. (76) and limiting the series expansion up to the maximum degree \bar{n} , we arrive at

$$\lim_{r \rightarrow R^-} V_i^{\delta\rho}(r, \Omega) = \frac{GM}{R} \sum_{n=0}^{\bar{n}} \sum_{m=-n}^n {}_iV_{n,m}^{\delta\rho} Y_{n,m}(\Omega), \tag{84}$$

where the potential coefficients ${}_iV_{n,m}^{\delta\rho}$ are given by

$${}_iV_{n,m}^{\delta\rho} = \frac{3}{2n+1} \frac{1}{\bar{\rho}_{\text{Earth}}} \sum_{i=0}^I \left({}_iFu_{n,m}^{(i)} - {}_iFl_{n,m}^{(i)} \right). \tag{85}$$

The numerical coefficients $\{ {}_iFl_{n,m}^{(i)}, {}_iFu_{n,m}^{(i)} : i = 0, 1, \dots, I \}$ in Eq. (86) read

$${}_iFl_{n,m}^{(i)} = \sum_{k=0}^{\infty} (-1)^k \binom{n+k-2}{k} \frac{1}{k+1+i} \frac{L_{n,m}^{(k+1+i)}}{R^{k+1}} \quad (i = 0, 1, \dots, I), \tag{86}$$

and

$${}_iFu_{n,m}^{(i)} = \sum_{k=0}^{\infty} (-1)^k \binom{n+k-2}{k} \frac{1}{k+1+i} \frac{U_{n,m}^{(k+1+i)}}{R^{k+1}} \quad (i = 0, 1, \dots, I). \tag{87}$$

References

Airy GB (1855) On the computations of the effect of the attraction of the mountain masses as disturbing the apparent astronomical latitude of stations in geodetic surveys. *Phil Trans Roy Soc (Lond) B* 145:101–104

- Allister NA, Featherstone WE (2001) Estimation of Helmert orthometric heights using digital barcode levelling, observed gravity and topographic mass-density data over part of Darling Scarp, Western Australia. *Geom Res Aust* 75:25–52
- Ardalan AA, Grafarend EW (1999) A first test for W_0 the time variation of W_0 based on three GPS campaigns of the Baltic Sea level project, final results of the Baltic Sea Level 1997 GPS campaign. *Rep Finnish Geod Inst* 99(4):93–112
- Årge J (2004) The analytical continuation bias in geoid determination using potential coefficients and terrestrial gravity data. *J Geod* 78:314–332
- Artemjev ME, Kaban MK, Kucherinenko VA, Demjanov GV, Taranov VA (1994) Subcrustal density inhomogeneities of the Northern Eurasia as derived from the gravity data and isostatic models of the lithosphere. *Tectonoph* 240:248–280
- Bagherbandi M, Tenzer R (2013) Geoid-to-quasigeoid separation computed using the GRACE/GOCE global geopotential model GOCO02S—a case study of Himalayas, Tibet and central Siberia. *Terr Atmo Ocean Sci* 24(1):59–68
- Bruns H (1878) *Die Figur der Erde*. Publ Preuss Geod Inst, Berlin
- Burke KF, True SA, Burša M, Raděj K (1996) Accuracy estimates of geopotential models and global geoids. In: Rapp RH, Cazenave AA, Nerem RS (eds) *Proceedings of symposium no 116 held in Boulder, CO, USA, July 12, 1995*. Springer, Berlin, pp 50–60
- Burša M, Radej K, Šíma Z, True SA, Vatr V (1997) Determination of the geopotential scale factor from TOPEX/POSEIDON satellite altimetry. *Stud Geoph Geod* 41:203–216
- Burša M, Kouba J, Kumar M, Müller A, Radej K, True SA, Vatr V, Vojtíšková M (1999) Geoidal geopotential and world height system. *Stud Geoph Geod* 43:327–337
- Burša M, Kouba J, Müller A, Raděj K, True SA, Vatr V, Vojtíšková M (2001) Determination of geopotential differences between local vertical datums and realization of a World Height System. *Stud Geoph Geod* 45:127–132
- Burša M, Kenyon S, Kouba J, Šíma Z, Vatr V, Vitek V, Vojtíšková M (2007) The geopotential value W_0 for specifying the relativistic atomic time scale and a global vertical reference system. *J Geod* 81(2):103–110
- Dayoub N, Edwards SJ, Moore P (2012) The Gauss-Listing geopotential value W_0 and its rate from altimetric mean sea level and GRACE. *J Geod* 86(9):681–694
- Dennis ML, Featherstone WE (2003) Evaluation of orthometric and related height systems using a simulated mountain gravity field. In: Tziavos IN (ed) *Gravity and geoid 2002*. Aristotle Univ Thessaloniki, Dept Surv Geod, Thessaloniki, pp 389–394
- Drewes H, Dodson AH, Fortes LP, Sanchez L, Sandoval P (eds) (2002) *Vertical reference systems*. IAG symposia 24. Springer, Berlin, p 353
- Featherstone WE (2013) Deterministic, stochastic, hybrid and band-limited modifications of Hotine's integral. *J Geod* 87(5):487–500
- Featherstone WE, Kuhn M (2006) Height systems and vertical datums: a review in the Australian context. *J Spatial Sci* 51(1):21–42
- Filmer MS, Featherstone WE, Kuhn M (2010) The effect of EGM2008-based normal, normal-orthometric and Helmert orthometric height systems on the Australian levelling network. *J Geod* 84(8):501–513
- Flury J, Rummel R (2009) On the geoid-quasigeoid separation in mountain areas. *J Geod* 83:829–847
- Goiginger H, Rieser D, Mayer-Guerr T, Pail R, Schuh W.-D., Jäggi A, Maier A (2011) GOCO, consortium: the combined satellite-only global gravity field model GOCO02S. European Geosciences Union General Assembly 2011, Vienna
- Grafarend EW, Ardalan AA (1997) W_0 : an estimate of the Finnish Height Datum N60, epoch 1993.4 from twenty-five GPS points of the Baltic Sea level project. *J Geod* 71(11):673–679
- Heiskanen WH, Moritz H (1967) *Physical geodesy*. WH Freeman and Co, San Francisco
- Helmert FR (1884) *Die mathematischen und physikalischen Theorien der höheren Geodäsie*, vol 2. Teubner, Leipzig
- Helmert FR (1890) *Die Schwerkraft im Hochgebirge, insbesondere in den Tyroler Alpen*. Veröff Königl Preuss Geod Inst, no 1
- Hinze WJ (2003) Bouguer reduction density, why 2.67? *Geophysics* 68(5):1559–1560
- Hirt C (2012) Efficient and accurate high-degree spherical harmonic synthesis of gravity field functionals at the Earth's surface using the gradient approach. *J Geod* 86(9):729–744
- Hofmann-Wellenhof B, Moritz H (2005) *Physical geodesy*, 2nd edn. Springer, Berlin
- Huang J, Vaníček P, Pagiatakis SD, Brink W (2001) Effect of topographical density on the geoid in the Rocky Mountains. *J Geod* 74:805–815
- Hwang C, Hsiao YS (2003) Orthometric height corrections from leveling, gravity, density and elevation data: a case study in Taiwan. *J Geod* 77(5–6):292–302

- Kao SP, Rongshin H, Ning FS (2000) Results of field test for computing orthometric correction based on measured gravity. *Geom Res Aust* 72:43–60
- Kingdon R, Vaníček P, Santos M (2009) Modeling topographical density for geoid determination. *Can J Earth Sci* 46(8):571–585
- Krakiwsky EJ (1965) Heights, MS thesis. Dept Geod Sci Surv, Ohio State Univ, Columbus, p 157
- Ledersteger K (1955) Der Schwereverlauf in den Lotlinien und die Berechnung der wahren Geoidschwere. Publication dedicated to Heiskanen WA, *Publ Finn Geod Inst*, No 46, pp 109–124
- Ledersteger K (1968) Astronomische und Physikalische Geodäsie (Erdmessung). In: Jordan W, Eggert E, Kneissl M (eds) *Handbuch der Vermessungskunde*, vol V. Metzler, Stuttgart
- Mader K (1954) Die orthometrische Schwerekorrektur des Präzisions-Nivellements in den Hohen Tauern. *Österreichische Zeitschrift für Vermessungswesen*, Sonderheft 15
- Marti U (2005) Comparison of high precision geoid models in Switzerland. In: Tregonig P, Rizos C (eds) *Dynamic planet*. Springer, Berlin
- Martinec Z (1998) Boundary value problems for gravimetric determination of a precise geoid. *Lecture notes in earth sciences*, vol 73. Springer, Berlin
- Meyer TH, Roman DR, Zilkoski DB (2007) What does height really mean? Part IV: GPS orthometric heighting. Department of Natural Resources and the Environment Articles, paper 5
- Molodensky MS (1945) *Fundamental Problems of Geodetic Gravimetry* (in Russian). TRUDY Ts NIIGAIK, 42, Geodezizdat, Moscow
- Molodensky MS (1948) External gravity field and the shape of the Earth surface (in Russian). *Izv CCCP*, Moscow
- Molodensky MS, Yeremeev VF, Yurkina MI (1960) Methods for study of the external gravitational field and figure of the earth. TRUDY Ts NIIGAIK, vol 131. Geodezizdat, Moscow. English translation: Israel Program for Scientific Translation, Jerusalem 1962
- Moritz H (1990) *Advanced physical geodesy*. Abacus Press, Tunbridge Wells
- Moritz H (2000) Geodetic reference system 1980. *J Geod* 74:128–162
- Niethammer T (1932) Nivellement und Schwere als Mittel zur Berechnung wahrer Meereshöhen. Schweizerische Geodätische Kommission
- Niethammer T (1939) Das astronomische Nivellement im Meridian des St Gotthard, Part II, Die berechneten Geoiderhebungen und der Verlauf des Geoidschnittes. *Astronomisch-Geodätische Arbeiten in der Schweiz*, vol 20. Swiss Geodetic Commission
- Novák P (2003) Geoid determination using one-step integration. *J Geod* 77:193–206
- Pavlis NK, Holmes SA, Kenyon SC, Factor JK (2012) The development and evaluation of the Earth Gravitational Model 2008 (EGM2008). *J Geophys Res* 117:B04406
- Pizzetti P (1911) Sopra il calcolo teorico delle deviazioni del geoido dall' ellissoide. *Atti R Accad Sci Torino* 46:331–350
- Pratt JH (1855) On the attraction of the Himalaya Mountains and of the elevated regions beyond upon the plumb-line in India, *Trans Roy Soc (Lond)*. B 145:53–100
- Rapp RH (1961) The orthometric height. M.S. Thesis, Dept Geod Sci, Ohio State Univ, Columbus, USA, p 117
- Rapp RH (1997) Use of potential coefficient models for geoid undulation determinations using a spherical harmonic representation of the height anomaly/geoid undulation difference. *J Geod* 71(5):282–289
- Sanchez L (2007) Definition and realisation of the SIRGAS vertical reference system within a globally unified height system. In: Tregonig P, Rizos C (eds) *Dynamic planet: monitoring and understanding a dynamic planet with geodetic and oceanographic tools*, IAG Symposia, vol 130, pp 638–645
- Santos MC, Vaníček P, Featherstone WE, Kingdon R, Ellmann A, Martin B-A, Kuhn M, Tenzer R (2006) The relation between rigorous and Helmert's definitions of orthometric heights. *J Geod* 80:691–704
- Sjöberg LE (1995) On the quasigeoid to geoid separation. *Manuscr Geod* 20(3):182–192
- Sjöberg LE (2006) A refined conversion from normal height to orthometric height. *Stud Geophys Geod* 50:595–606
- Sjöberg LE (2007) The topographical bias by analytical continuation in physical geodesy. *J Geod* 81:345–350
- Sjöberg LE (2010) A strict formula for geoid-to-quasigeoid separation. *J Geod* 84:699–702
- Sjöberg LE (2012) The geoid-to-quasigeoid difference using an arbitrary gravity reduction model. *Stud Geophys Geod* 56:929–933
- Sjöberg LE, Bagherbandi M (2012) Quasigeoid-to-geoid determination by EGM08. *Earth Sci Inform* 5:87–91
- Somigliana C (1929) *Teoria Generale del Campo Gravitazionale dell'Ellissoide di Rotazione*. Milano, Memoire della Societa Astronomica Italiana, p 425

- Strange WE (1982) An evaluation of orthometric height accuracy using borehole gravimetry. *Bull Géod* 56:300–311
- Sünkel H (1986) Digital height and density model and its use for the orthometric height and gravity field determination for Austria. In: Proceedings of the international symposium on the definition of the geoid, Florence, Italy, May, pp 599–604
- Sünkel H, Bartelme N, Fuchs H, Hanafy M, Schuh WD, Wieser M (1987) The gravity field in Austria. In: Austrian Geodetic Commission (ed) The gravity field in Austria. *Geodätische Arbeiten Österreichs für die Internationale Erdmessung, Neue Folge*, vol IV, pp 47–75
- Tenzer R (2004) Discussion of mean gravity along the plumbline. *Stud Geoph Geod* 48:309–330
- Tenzer R, Novák P (2008) Conditionality of inverse solutions to discretized integral equations in geoid modelling from local gravity data. *Stud Geoph Geod* 52:53–70
- Tenzer R, Vaníček P (2003) Correction to Helmert's orthometric height due to actual lateral variation of topographical density. *Rev Brasil Cartogr* 55(02):44–47
- Tenzer R, Vaníček P, Santos M, Featherstone WE, Kuhn M (2005) The rigorous determination of orthometric heights. *J Geod* 79(1–3):82–92
- Tenzer R, Moore P, Novák P, Kuhn M, Vaníček P (2006) Explicit formula for the geoid-to-quasigeoid separation. *Stud Geoph Geod* 50:607–618
- Tenzer R, Vatrt V, Abdalla A, Dayoub N (2011a) Assessment of the LVD offsets for the normal-orthometric heights and different permanent tide systems—a case study of New Zealand. *Appl Geomat* 3(1):1–8
- Tenzer R, Vatrt V, Luzi G, Abdalla A, Dayoub N (2011b) Combined approach for the unification of levelling networks in New Zealand. *J Geod Sci* 1(4):324–332
- Tenzer R, Sirguey P, Rattenbury M, Nicolson J (2011c) A digital bedrock density map of New Zealand. *Comput Geosci* 37(8):1181–1191
- Tenzer R, Novák P, Vajda P, Gladkikh V, Hamayun (2012a) Spectral harmonic analysis and synthesis of Earth's crust gravity field. *Comput Geosci* 16(1):193–207
- Tenzer R, Gladkikh V, Vajda P, Novák P (2012b) Spatial and spectral analysis of refined gravity data for modelling the crust-mantle interface and mantle-lithosphere structure. *Surv Geophys* 33(5):817–839
- Tziavos IN, Featherstone WE (2001) First results of using digital density data in gravimetric geoid computation in Australia. In: Sideris MG (ed) *Gravity, geoid and geodynamics 2000*. Springer, Berlin, pp 335–340
- Vaníček P, Kingdon (2012) Geoid versus quasigeoid: A case of physics vs geometry. *Contrib Geophys Geod* 42(1):101–118
- Vaníček P, Kleusberg A, Martinec Z, Sun W, Ong P, Najafi M, Vajda P, Harrie L, Tomášek P, Horst B (1995) Compilation of a precise regional geoid. Final report on research done for the Geodetic Survey Division, Fredericton
- Vaníček P, Tenzer R, Sjöberg LE, Martinec Z, Featherstone WE (2005) New views of the spherical Bouguer gravity anomaly. *Geophys J Int* 159:460–472
- Vermeer M (2008) Comment on Sjöberg (2006) “The topographic bias by analytical continuation in physical geodesy”. *J Geod* 81(5):345–350. *J Geod* 82:445–450
- Wirth B (1990) Höhensysteme, Schwerepotentiale und Niveauflächen. *Geodätisch-Geophysikalische Arbeiten in der Schweiz*, vol 42. Swiss Geodetic Commission